SUMMARY

A DWBA ANALYSIS OF ^{9}BE (P,D) ^{8}BE

John L. Schoonover
M. Sc. Physics

The ^{9}Be (p,d) ^{8}Be reaction at incident proton energies of 46 Mev and 100 MeV has been analyzed using the DWBA theory. The finite-range approximation has been used. The transferred neutron was assumed to be bound by a Woods-Saxon potential in the target nucleus. The proton distorted waves were generated using the optical potential obtained from elastic scattering from ^{9}Be, while the deuteron optical potential was obtained by fitting the angular distribution of the ground state transition in the reaction. Transitions to the excited states were analyzed with all potential parameters fixed. Fairly good agreement with experiment has been obtained. The spectroscopic factors extracted from the experiment were compared with previous work as well as with the predictions of various nuclear models. Large discrepancies between the experiments and the predictions of intermediate coupling shell model were found, especially in the high-lying states. The cluster model provided a qualitative explanation of the present results.

A DWBA ANALYSIS OF ^{9}BE (P,D) ^{8}BE

by

JOHN L. SCHOONOVER, B. A.

A thesis submitted to the Faculty of Graduate Studies and Research in partial fulfillment of the requirements for the degree of Master of Science.

Foster Radiation Laboratory
McGill University, Montreal

July, 1969

ABSTRACT

The ^{9}Be (p,d) ^{8}Be reaction at incident proton energies of 46 MeV and 100 MeV has been analyzed using the DWBA theory. The finite-range approximation has been used. The transferred neutron was assumed to be bound by a Woods-Saxon potential in the target nucleus. The proton distorted waves were generated using the optical potential obtained from elastic scattering from ^{9}Be, while the deuteron optical potential was obtained by fitting the angular distribution of the ground state transition in the reaction. Transitions to the excited states were analyzed with all potential parameters fixed. Fairly good agreement with experiment has been obtained. The spectroscopic factors extracted from the experiment were compared with previous work as well as with the predictions of various nuclear models. Large discrepancies between the experiments and the predictions of intermediate coupling shell model were found, especially in the high-lying states. The cluster model provided a qualitative explanation of the present results.

ACKNOWLEDGEMENTS

I am deeply indebted to Dr. S. K. Mark, my research director, for his guidance during the completion of this work. Also, thanks are due to Dr. T. Y. Li, who developed the computer codes used in the analysis. Many hours of fruitful discussion were spent with both of these gentlemen.

I am grateful to Professor R. E. Bell, Director of the Foster Radiation Laboratory, and to the Atomic Energy Control Board of Canada for financial support during part of this work. For support during the remainder, I would like to thank the National Research Council.

For the use of their facilities, I would like to thank the McGill Computing Center.

For their help on many of the mechanical aspects of putting the thesis together, I would like to thank Mrs. Robert Egan, typist, Mr. Stanley Garber, who did most of the drawings, and Miss Peggy Simpson, who helped to collate the copies.

TABLE OF CONTENTS

	Page
Abstract	i
Acknowledgements	ii
List of Figures	iv
List of Tables	vi
1. Introduction	1
2. Formalism	6
2.1 DWBA Differential Cross Section	6
2.2 Antisymmetrization	14
2.3 Formalism in the JT Representation	16
2.4 The Spectroscopic Factor in the Shell Model JT Representation	25
3. Methods of Numerical Computation	32
3.1 The Radial Integral	32
3.2 The Distorted Waves	33
3.3 The Bound State Neutron Wave Function	36
3.4 The Zero-Range Approximation	37
3.5 The Finite-Range Approximation	39
4. Analysis of the Reaction ^{9}Be (p,d) ^{8}Be	42
4.1 Method of Analysis	42
4.2 Results and Comparison with the Experiments	55
5. Conclusion	102
References	105
Appendices	108
A. Simplification of $\|T_{if}\|^2$	108
B. Use of the DWBA Computer Code	109

LIST OF FIGURES

Figure	Title	Page
1	The coordinates of a system of particles in the center-of-mass system for a (p,d) or a (d,p) reaction	18
2	A partial diagram of the known energy levels of ^{8}Be	46
3	Optical model fitting of the 46 MeV elastic scattering data	53
4	Angular distribution for the ground state transition, showing the fit obtained by using potential $46W_V$	57
5	Angular distribution for the ground state transition, showing the fit obtained by using potential $46W_D$	59
6	Angular distribution for the ground state transition, showing the fit obtained by using potential $100W_V$	61
7	Angular distribution for the ground state transition, showing the fit obtained by using potential $100W_D$	63
8	Angular distribution for the 2.9 MeV state transition, showing the fit obtained by using potential $46W_V$	67
9	Angular distribution for the 2.9 MeV state transition, showing the fit obtained by using potential $46W_D$	69
10	Angular distribution for the 16.93 MeV state transition, showing the fit obtained by using potential $46W_V$	71
11	Angular distribution for the 16.93 MeV state transition, showing the fit obtained by using potential $46W_D$	73
12	Angular distribution for the 17.64 MeV state transition, showing the fit obtained by using potential $46W_V$	75
13	Angular distribution for the 17.64 MeV state transition, showing the fit obtained by using potential $46W_D$	77

14	Angular distribution for the 18.15 MeV state transition, showing the fit obtained by using potential $46W_V$	79
15	Angular distribution for the 18.15 MeV state transition, showing the fit obtained by using potential $46W_D$	81
16	Angular distribution for the 19.05 MeV state transition, showing the fit obtained by using potential $46W_V$	83
17	Angular distribution for the 19.05 MeV state transition, showing the fit obtained by using potential $46W_D$	85
18	Angular distribution for the 2.9 MeV state transition, showing the fit obtained by using potential $100W_V$	87
19	Angular distribution for the 2.9 MeV state transition, showing the fit obtained by using potential $100W_D$	89
20	Angular distribution for the 16-20 MeV states transitions, showing the fit obtained using potential $100W_V$	91
21	Angular distribution for the 16-20 MeV states transitions, showing the fit obtained using potential $100W_D$	93

LIST OF TABLES

Table	Title	Page
4-1	Differential cross sections for ^{9}Be (p,d) ^{8}Be at 46 MeV	43
4-2	Differential cross sections for ^{9}Be (p,d) ^{8}Be at 100 MeV	45
4-3	Neutron potential parameters	49
4-4	Proton channel optical parameters from ^{9}Be (p,p) ^{9}Be	52
4-5	Deuteron channel optical parameters form ^{9}Be (p,d) ^{8}Be	65
4-6	Spectroscopic factors extracted in this work, compared to theoretical results	97
4-7	Spectroscopic factors extracted in this work	98
4-8	Spectroscopic factors extracted by Towner (1969)	101

CHAPTER 1

INTRODUCTION

For a long time nuclear pick-up and stripping reactions have been among the principal tools of nuclear physics. Among other uses, these reactions are important in the determination of spectroscopic data such as nuclear spins and parities and energy level schemes. They are also useful in testing nuclear models and determining nuclear wave functions. The latter two uses will be of main interest in this thesis.

Nuclear reactions are generally characterized by the bombardment of a target A by a projectile a with the result that a residual nucleus B and an outgoing particle b are produced. In abbreviated notation this can be written A(a,b)B. In this work the primary interest is with the pick-up reaction (p,d) which is closely related to the time-reversed reaction, that is the (d,p) stripping reaction.

It is possible to classify nuclear reactions further as due to compound nucleus or direct processes. A compound nucleus reaction occurs if the incident particle is absorbed by the target and undergoes multiple internal collisions with the individual particles of the target. The multiple scattering causes the incident particle to forget its history, in a sense, which causes the differential cross section to have a much different angular dependence

from that associated with direct reactions. It has been found that for compound nuclear reactions it is difficult to calculate matrix elements for the scattering, since the properties of the intermediate states are very poorly understood. On the other hand, calculations for direct reactions have been done with increasing sophistication and more gratifying results since at least the early 1950's. By comparison to the compound reaction, the direct reaction is very simple. The incident projectile is in the region of the target for a short time and interacts with very few of the target nucleons. Since there are no intermediate states formed, the matrix elements involve only the states of the initial and final nuclei and the interaction responsible for the reaction.

In the early 1950's Butler (1957) proposed a method for calculating the reaction matrix elements which had the virtues of being within the capabilities of the calculating facilities available at the time and yielded values in fair agreement with experiments. With the Butler theory it was possible to determine the orbital angular momentum transfer with a fair degree of certainty. This in turn enabled investigators to determine spins and parities of numerous states. The Butler theory has the draw back, that it often overestimates the differential cross section by as much as an order of magnitude, and does not give good shape fitting at large angles. Some of this difficulty can be attributed to the use of the

plane wave approximation for the incident and outgoing particles. With the advent of high speed computers in the late 1950's, it became practical to use the distorted waves approximation for the incident **and** outgoing particles. Since that time numerous improvements have been made in the methods for calculating the matrix elements. Among these is the finite-range approximation, which will be discussed in some detail.

Among the 1p shell nuclei much work has been done to determine the ground state wave function and spectroscopic factors for various pick-up and stripping reactions (Cohen and Kurath, 1967; Kull, 1967; Mac Farlane and French, 1960; Li and Mark, 1969a, 1969b; Towner, 1969; Verba, 1967; Marion, 1965; Marion et al., 1966; Wildermuth, 1962; Jacmart, 1964). Usually one assumes a model for the nucleus and tries to make up the wave function which predicts energy levels with the correct quantum numbers, for instance. The same wave function can then be used to calculate spectroscopic factors which are consistent with the assumed model. This is essentially the program followed by Cohen and Kurath (1967) in their calculations. Since their table became available, a number of investigators have used it as a guide in determining experimental spectroscopic factors over a wide range of energies (Kull, 1967; Li and Mark 1969a, 1969b; Towner, 1969; Verba, 1967).

This thesis is arranged into two distinct parts.

The first is concerned with the details of the reaction theory, and the second deals with the actual analysis of data from the ^{9}Be(p,d) ^{8}Be reaction at 46 MeV and 100 MeV. Chapters 2 and 3 comprise the first part, and they can be broken down further into two related problems. To begin with, the theory is developed step by step paying attention to the assumptions and the essential physics of the problem. The concept of the differential cross section is discussed, and the physical necessity of anti-symmetrization for systems of Fermions and the results of the process are presented. Afterward, the claculation is narrowed to the specific case of scattering between nucleons whose wave functions are given in the J T representation. At this point the necessity for spectroscopic factors becomes apparent and some of the methodology for calculating them in the J T representation is explained. Chapter 3 is devoted to the second problem, which is the practical difficulty of evaluating the transition matrix element. For any reasonable potential, neither the distorted waves nor the bound state neutron wave function can be written in closed form. For meaningful calculations, then, one must rely on the methods of numerical calculus.

The analysis section, Chapter 4, involves fitting ^{9}Be(p,d) ^{8}Be angular distributions using distorted waves for both the proton and deuteron generated with optical potentials. The quality of the fits is discussed, and experimental spectroscopic factors are extracted for the

ground, 2.90, 16.93, 17.64, 18.15, and 19.05 MeV states. These values are compared to those extracted by Kull (1967) at 33.6 MeV and Towner (1969) at 155 MeV. In addition, they are compared to the theoretical values given by Cohen and Kurath (1967) and Balashov et al. (1965) based on the intermediate coupling shell model. In this section, several models for ^{9}Be are discussed and their merits are considered in light of the results of this work.

CHAPTER 2

FORMALISM

2.1 DWBA Differential Cross Section

Calculation of a differential cross section involves the evaluation of a matrix element made up of a wave function which describes the state of the complete system, an effective interaction potential, and the final state of the outgoing particle and the residual nucleus with no interaction between them. In the simplest derivation of the expression for the differential cross section, it is necessary to assume that the asymptotic form of the potential is proportional to r^{-n}, where $n \geq 2$. However, for scattering of charged particles, this is obviously not a good assumption, since the Coulomb potential has r^{-1} dependence. The derivation using time dependent perturbation theory (Gell-Mann and Goldberger, 1953) is free from this restriction, and gives the same result to first order as does the more restricted derivation. This is because the Coulomb interaction is relatively weak compared to the nuclear interactions.

The basic assumption of the time dependent perturbation approach is that the Hamiltonian of a system of nucleons can be written in such a way that the interaction between incident and target nuclei appears as a perturbation. The main part of the Hamiltonian describes the internal motion of target and projectile. By a heuristic argument

it is easy to show that the interaction energy is small compared to the energy of internal motion of the target, and hence, can be used as a perturbation. A proton, for instance, interacts with a target of A nucleons; the A nucleons interact among themselves by A! nucleon-nucleon combinations. Since the energy of each nucleon-nucleon interaction should be of nearly the same magnitude, that portion due to the internal motion would be of the order of (A-1)! greater than that due to the proton.

In the case of the (p,d) reaction, in which a neutron in the target nucleus is transferred to the outgoing particle, the Hamiltonian can be written for the incident proton channel as

$$H = H_p + V. \qquad (2\text{-}1)$$

The first term, Hp, includes the interaction of the A-1 nucleons, called the core, among themselves, the interaction of a bound neutron with the nucleons of the core and the relative motion between the incoming proton and the target nucleus. A less model-dependent description of Hp is that it describes the interaction of the A target nucleons and the relative motion of the projectile and the target. More important than this term is the second term, V, which appears in the matrix element for the differential cross section. V describes the interaction of the incoming proton with the A target nucleons in such a way that the interaction with the neutron to be picked up appears

separately.

$$V = V_{pc} + V_{pn} \tag{2-2}$$

Here, V_{pc} is the interaction between the incoming proton and the core, and V_{pn} is the interaction between the proton and the transferred target neutron. One can write a similar expression for the Hamiltonian for the outgoing deuteron channel.

$$H = H_d + U \,, \quad U = V_{pc} + V_{nc} \tag{2-3}$$

Here the internal motion of the deuteron, the A-1 nucleons in the residual nucleus, and their relative motion are lumped in the unperturbed part, H_d, and the interactions of the proton and neutron with the residual nucleus are considered separately and given by U. By the law of conservation of energy, the Hamiltonian of the complete system is

$$H = H_p + V_{pc} + V_{pn} = H_d + V_{pc} + V_{nc} \tag{2-4}$$

Gell-Mann and Goldberger (1953) given an expression for the transition rate per unit time per unit final system.

$$\omega_{if} = \frac{2\pi}{\hbar} \left| \langle \Phi_d | V_{pc} + V_{pn} | \psi_p^{(+)} \rangle \right|^2 \delta(E_i - E_f) \tag{2-5}$$

Here, $\psi_p^{(+)}$ is the exact-state vector given by the Schrödinger equation

$$(H - E)\,\psi = 0 \tag{2-6}$$

With the boundary condition that the solution contains outgoing spherical proton waves at infinity; Φ_d is the

wave function for the final system consisting of the outgoing deuteron and the residual nucleus with no interaction between them and satisfies the Schrödinger equation

$$(H_d - E)\Phi_d = 0 \tag{2-7}$$

The delta function in energy of the initial and final channels expresses the conservation of energy in the reaction. In order to find the transition probability per unit time, introduce $\rho(E_f)$, the number of final states per unit final energy interval in an energy region around E_f. After integrating over the final energy E_f, the transition probability per unit time is

$$P_{if} = \frac{2\pi}{\hbar}\left|\langle \Phi_d | V_{pC} + V_{pn} | \psi_p^{(+)} \rangle\right|^2 \rho(E_f). \tag{2-8}$$

For particles with energy $p^2/2m$, the number of states in a volume element of phase space is

$$dN = \frac{p^2 dp\, d\Omega}{(2\pi\hbar)^3} \tag{2-9}$$

The momentum p of the particles lies in the direction between solid angle Ω and $\Omega+d\Omega$, and the geometrical space volume is unity. The number of states in the energy interval E to E+dE is

$$\rho(E) = \frac{dN}{dE} = \frac{mp\, d\Omega}{(2\pi\hbar)^3}. \tag{2-10}$$

The quantities m and p are respectively the reduced mass of the outgoing particle from the reaction and the momentum of this particle. P_{if}, which is the probability per unit time for a transition from the initial to the final state, can be thought of as the flux of final state particles.

In order to convert this expression into a differential cross section, it is necessary to consider the incident particle current intensity. If the incident beam is normalized to a density of one unit per unit volume, and if $\bar{v}_i$ is the velocity of the particles, the incident particle beam intensity is v_i. Then, the differential cross section is defined by

$$d\sigma = \frac{P_{if}}{v_i}, \tag{2-11}$$

which leads to the expression

$$\frac{d\sigma}{d\Omega} = \frac{\mu_i \mu_f}{(2\pi\hbar^2)^2} \frac{k_f}{k_i} \left| \langle \varphi_d | V_{pc} + V_{pn} | \psi_p^{(+)} \rangle \right|^2, \tag{2-12}$$

where k_i and k_f are the wave numbers for the incident and outgoing particles, and μ_i and μ_f are the reduced masses.

Throughout the derivation, there has been an assumption that the particles are spinless. If this is not the case, and in addition, neither the incident nor the outgoing particles are polarized, it is necessary to average the cross section over incident spin states of the target and projectile and sum over final spin states of the residual nucleus and detected particle. If J_i, M_i and J_f, M_f are angular momentum quantum numbers for target and residual nuclei and s_i, m_i and s_f, m_f are used for the incident and outgoing particle spins, the differential cross section can immediately be written as follows:

$$\frac{d\sigma}{d\Omega} = \frac{\mu_i \mu_f}{(2\pi\hbar^2)^2} \frac{k_f}{k_i} \frac{1}{(2J_i+1)(2s_i+1)} \sum_{\substack{M_i M_f \\ m_i m_f}} \left| \langle \varphi_d | V_{pc} + V_{pn} | \psi_p^{(+)} \rangle \right|^2. \tag{2-13}$$

The quantity $\langle \varphi_d | V_{pc} + V_{pn} | \psi_p^{(+)} \rangle$, denoted by T_{if} and called the transition amplitude is the crux of the scattering problem. The evaluation of the transition matrix element, T_{if}, is not an easy task because it contains $\psi_p^{(+)}$, the exact solution of equation (2-6) with the prescribed boundary condition. An approximation must be made here. It has been shown by Feshbach (1958) and Glendenning (1963) that the potential V_{pc} can be approximated by an optical potential V_p, and the wave function $\psi_p^{(+)}$ by $\chi_p^{(+)}$, the optical wave function solution of the Schrödinger equation

$$(H_p + V_p - E)\chi_p = 0 \qquad (2\text{-}14)$$

with the boundary condition that it contains outgoing spherical proton waves. Similarly, $U = V_{pc} + V_{nc}$ is approximated by a deuteron optical potential V_d and φ_d is replaced by $\chi_d^{(-)}$, the optical wave function containing incoming spherical deutron waves given by

$$(H_d + V_d - E)\chi_d = 0 \qquad (2\text{-}15)$$

This method of evaluating T_{if} is called the distorted - wave - Born - approximation or DWBA (Tobocman, 1961). The spherical wave boundary conditions can be explained by comparison to the plane - wave - Born - approximation (PWBA). In this case the incident particle is assumed to be free and its motion is described by a plane wave. There is also a scattered component given by spherical waves emitted from the scattering center. In the infinite

limit one would expect DWBA and PWBA wave functions to have the same form, since the distorted wave particle is free by the time it travels a large distance. The outgoing particle channel is the time reversed analog of an incoming particle channel. Hence, the asymptotic behavior is time reversed, that is the spherical wave is coming in toward the scattering center. It is important to keep in mind that, due to the presence of H_p and H_d, these wave functions also contain the internal structure of the systems of A and A-1 nucleons.

In deriving the optical model wave functions, $\chi_p^{(+)}$ and $\chi_d^{(-)}$, two important operators were used. These are the projection operator P, which when used on an arbitrary wave function of a system projects out only the ground state, and its complementary operator Q, which projects out the excited state components of the wave function. The optical wave function $\chi_d^{(-)}$ defined in equation 2-15 is generated in such a way, that it is a pure ground state wave function. It will be shown later that $\chi_p^{(+)}$, as defined in equation 2-14 contains a component corresponding to $\chi_d^{(-)}$. In the meantime, the transition amplitude can be written as

$$T_{if} \simeq \langle \chi_d^{(-)} | U + V_{pn} | \chi_p^{(+)} \rangle \tag{2-16}$$

$$U = Q(V_{pc})Q + P(V_{pc})Q + Q(V_{pc})P. \tag{2-17}$$

This expression reduces immediately to

$$T_{if} \simeq \langle \chi_d^{(-)} | V_{pn} + Q(V_{pc})P | \chi_p^{(+)} \rangle. \tag{2-18}$$

This is the transition amplitude in DWBA.

Physically, the reaction theory as formulated above assumes the validity of the optical model for predicting the results of elastic scattering. In order to generate inelastic matrix elements, a perturbation is introduced, which picks out other exit channels for the reaction.

The theory outlined above has been given for (p,d) reaction, in which a neutron is transferred from the target to the incoming projectile. However, because of time reversal invariance of nuclear reactions, the transition matrix for (d,p) reaction leading from the state f to the state i has the same value as that for (p,d) reaction from state i to state f (Messiah, 1966):

$$\langle \Phi_d | V_{pn} + Q V_{pc} P | \Psi_p^{(+)} \rangle^{+} = \langle \Phi_p | V_{pn} + Q V_{pc} P | \Psi_d^{(+)} \rangle, \quad (2\text{-}19)$$

or

$$\langle \chi_d^{(-)} | V_{pn} + Q V_{pc} P | \chi_p^{(+)} \rangle^{+} = \langle \chi_p^{(-)} | V_{pn} + Q V_{pc} P | \chi_d^{(+)} \rangle.$$

From the principle of detailed balance (Blatt and Weisskopf, 1952), one can write the differential cross section for (d,p) reaction in terms of (p,d) differential cross section:

$$\left(\frac{d\sigma}{d\Omega}\right)_{dp} = \left(\frac{k_p}{k_d}\right)^2 \frac{(2J_p+1)(2s_p+1)}{(2J_d+1)(2s_d+1)} \left(\frac{d\sigma}{d\Omega}\right)_{pd}. \quad (2\text{-}20)$$

J_p and J_d are the spin of the nucleus in the proton and deuteron channels; s_p and s_d are the proton and deuteron spins, $\frac{1}{2}$ and 1; k_p and k_d are the proton and deuteron momenta in units of $\hbar$ in the centre - of - mass - systems, respectively.

For the sake of convenience the calculation

performed hereafter will be done for the (d,p) reaction. This is done mainly because the computer code was written for (d,p) matrix element calculation.

2.2 Antisymmetrization

The idea of a target nucleus and a separate particle called an incident projectile are convenient fictions introduced to help the physicists to describe the interaction process. To be more accurate, it is necessary to think of the reaction involving so many identical fermions. In such a case, the incident and final state wave functions must be totally antisymmetrized. Consider a stripping process, (d,p), in which a deuteron impinging upon a target nucleus of A nucleons and transferring a neutron to the target, the initial system consists of two groups of 2 and A fermions and the final system comprises of two groups of 1 and A + 1 fermions. If one writes the initial and final wave functions, $\chi_d^{(+)}$ and $\chi_p^{(-)}$, as product wave functions of the internal motion of each group and the relative motion between groups, one must antisymmetrize the complete wave function with respect to interchange of particles between groups. The total number of permutations in the system is $(A + 2)!$, and the number of permutations which do not lead to new wave functions is $A!\,2!$ in the deuteron channel and $(A + 1)!1!$ in the proton channel. Hence, there are $N_i=(A + 2)!/A!2!$ and $N_f=(A + 2)!/(A + 1)!1!$ terms of product wave functions in the totally antisymmetrized.

initial and final wave functions, respectively. The transition matrix, T_{if}, given in equation (2-19) becomes

$$T_{if} = \frac{1}{\sqrt{N_i N_f}} \langle \mathcal{A} \chi_p^{(-)} | V_{pn} + Q V_{pc} P | \mathcal{A} \chi_d^{(+)} \rangle \qquad (2\text{-}21)$$

where $\mathcal{A} \chi_d^{(+)}$ and $\mathcal{A} \chi_p^{(-)}$ are the totally antisymmetrized initial and final wave functions. In the argument presented above, it is implicitly assumed that protons and neutrons are identical particles. To a good approximation this is true in the isotopic spin formalism. Throughout the calculation the isotopic spin formalism will be used, and its importance will become more apparent in later sections of this paper.

Consider the general case of an a-particle projectile incident on an A-particle target with one particle stripped. This leaves an (a - 1)-particle outgoing projectile and an (A + 1)-particle residual nucleus. The antisymmetization gives $N_i = (A + a)!/A!\, a!$ and $N_f = (A + a)!/(A + 1)!(a - 1)!$ with the transition given by (2-21) unchanged in form. The total number of terms in T_{if} is equal to the number of products between the initial and final state wave functions;

$$\frac{(A+a)!\,(A+a)!}{A!\,(A+1)!\,a!\,(a-1)!}\,.$$

In order for one of these products to be non-vanishing, the nucleons left in the core of the residual nucleus (comprising the initial target nucleus) must match the nucleons of the target nucleus.

Suppose for a particular term in the initial

state wave function particles labeled x, y, and z appear in the incident projecticle function, and the target is comprised of particles labeled a, b, and c. There will be terms of the final state wave function with the outgoing projectile containing particles labeled xy, xz, and yz, as well as others containing only one or none of x, y, and z. The residual nucleus terms corresponding to the outgoing particles listed above contain abcz, abcy, and abcx. Non-vanishing terms of the overlap integral occur when particles x, y, and z are decoupled from abc and in no other cases for this particular term of the initial state wave function. It is seen that this gives three terms, which is the number of nucleons in the incident projectile. By carrying this argument to an a-particle projectile, it is found that the number of non-vanishing products for each term of the initial wave function is a. Hence, the antisymmetrized transition amplitude is arrived at when the unsymmetrized one is multiplied by the normalizations $N_i^{-\frac{1}{2}}$ and $N_f^{-\frac{1}{2}}$ and the number of non-vanishing products, that is $(N_i N_f)^{-\frac{1}{2}} a(A + a)!/A!a! = a(A + 1)$.

2.3 Formalism in the J T Representation

Combining the results of DWBA, equation 2-18, and antisymmetrization, equation 2-13 becomes

$$\frac{d\sigma}{d\Omega} = \frac{\mu_i \mu_f}{(2\pi\hbar^2)^2} \frac{k_f}{k_i} \frac{a(A+1)}{(2J_i+1)(2s_i+1)} \sum_{\substack{M_i M_f \\ m_i m_f}} \left| \langle \chi_p^{(-)} | V_{pn} + Q(V_{pc})P | \chi_d^{(+)} \rangle \right|^2 . \quad (2\text{-}22)$$

In order to further specify the optical model wave functions $\chi_p^{(-)}$ and $\chi_d^{(+)}$, it is necessary to introduce a set of coordinate axes. The most convenient set, since the particle coordinate can be written in separable fashion, and the conventional set is the center - of - mass axes. Figure 1a shows the coordinates of the system of particles in the center - of - mass system for the deuteron channel, and Figure 1b shows the coordinates for the proton channel. The three vectors $\bar{r}_p$, $\bar{r}_n$, and $\bar{R}$ are directed from the center - of - mass of the target, A, to the proton and neutron of the incident deuteron and to the center - of - mass of the deuteron, In Figure 1b, the analogous vectors $\bar{r}_p'$, $\bar{r}_n'$, and $\bar{R}'$ are directed from the center - of - mass of the residual nucleus. Of the two remaining vectors, $\bar{r}$ gives the relative proton - neutron positions, both before and after the neutron is stripped, and $\bar{r}_a$ is the distance between the center - of - mass of A and A + 1 nucleons. At a later stage of the calculation, the origin will be shifted as a matter of convenience in numerical evaluation. By using the definition of center - of - mass and the construction of the diagrams, certain useful relations are found.

$$\bar{r} = \bar{r}_n - \bar{r}_p = \bar{r}_n' - \bar{r}_p' \tag{2-23}$$

$$\bar{R} = \tfrac{1}{2}(\bar{r}_p + \bar{r}_n) \tag{2-24}$$

$$\bar{R}' = \tfrac{1}{2}(\bar{r}_p' + \bar{r}_n') = \bar{R} - \frac{m_n}{m_A}\bar{r}_n' \tag{2-25}$$

FIGURE 1

The coordinates of a system of particles in the center-of-mass system for a (p,d) or a (d,p) reaction. The deuteron channel is exhibited in part a, and the proton channel in part b.

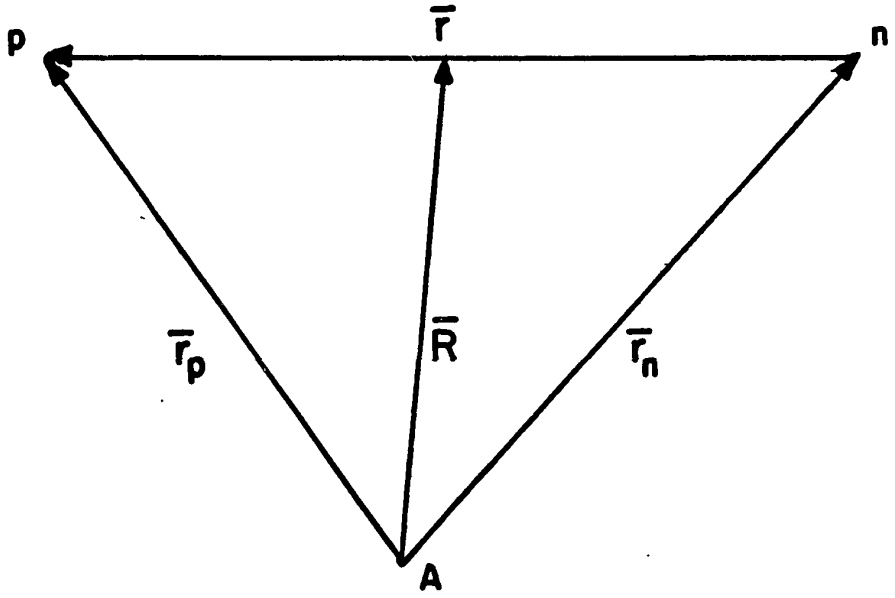

(a)

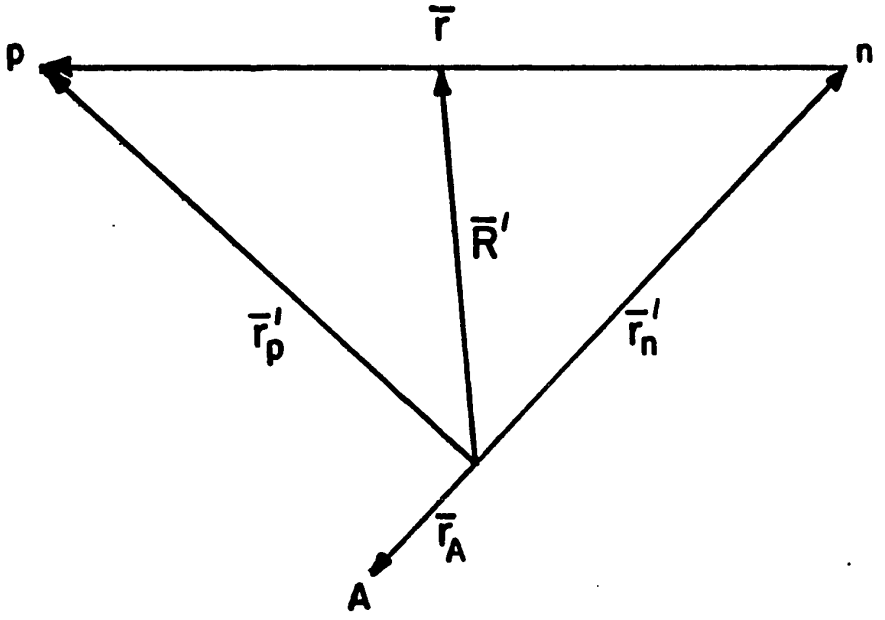

(b)

$$\bar{r}_n = \frac{m_A + m_n}{m_A} \bar{r}_n' \qquad (2\text{-}26)$$

The masses used in equations 2-25 and 2-26 are the target, m_A, and a nucleon, m_n.

In the J T representation, the distorted waves which appear in the transition matrix for the (d,p) reaction are written as follows (Glendenning, 1963):

$$\chi_d^{(+)} = \psi_d^{(+)}(\bar{r}_d, \bar{R})\, \phi_d(\bar{r})\, \chi_1^{\mu_d}\, \tau_0^{\nu_d}\, \Psi_{J_i T_i}^{M_i}(A) \qquad (2\text{-}27)$$

$$\chi_p^{(-)} = \psi_p^{(-)}(\bar{r}_p, \bar{R}_p')\, \chi_{\nu_2}^{\mu_p}\, \tau_{1/2}^{\nu_p}\, \Psi_{J_f T_f}^{M_f}(A+1) \qquad (2\text{-}28)$$

The functions $\psi_d^{(+)}$ and $\psi_p^{(-)}$ describe the motion of the deuteron and proton as particles undergoing elastic scattering by a central optical potential appropriate to the channel in question. The form of the potentials will be discussed in more detail later.

Internal structure of the target and residual nuclei is contained in the functions $\Psi_{J_i T_i}^{M_i}(A)$ and $\Psi_{J_f T_f}^{M_f}(A+1)$. The various indices represent the number of nucleons (A, A + 1), the nuclear spin (J_i, J_f) and z-component (M_i, M_f), and the isospin (T_i, T_f). The remaining wave functions in equations 2-27 and 2-28 describe the proton and deuteron. Specifically, the spins are contained in $\chi_1^{\mu_d}$, and $\chi_{\nu_2}^{\mu_p}$, the isospins in $\tau_0^{\nu_d}$ and $\tau_{1/2}^{\nu_p}$ and the deuteron internal spatial wave function in $\phi_d(\bar{r})$. For the deuteron, the wave functions are written explicitly as follows (Nigam and Roy, 1967):

$$\chi_1^{\mu_d} = \sum_{\mu_s, \mu_p} \left\langle \tfrac{1}{2}\mu_p\, \tfrac{1}{2}\mu_s \,||\, \mu_d \right\rangle \chi_{1/2}^{\mu_s}\, \chi_{1/2}^{\mu_p} \qquad (2\text{-}29)$$

$$\tau_0^0 = \langle \tfrac{1}{2} -\tfrac{1}{2} \tfrac{1}{2} \tfrac{1}{2} | 00 \rangle \left[\tau_{1/2}^{-\frac{1}{2}}(1)\, \tau_{1/2}^{1/2}(2) - \tau_{1/2}^{1/2}(1)\, \tau_{1/2}^{-1/2}(2) \right] \qquad (2\text{-}30)$$

$$\varphi_d(r) = \frac{1}{\beta - \alpha} \left\{ \frac{\alpha\beta(\alpha+\beta)}{2\pi} \right\}^{1/2} \frac{e^{-\alpha r} - e^{-\beta r}}{r} \qquad (2\text{-}31)$$

In equation 2-31, the quantities α and β are constants characteristic of the Hulthén potential and the Hulthén wave function for the deuteron (Buttle and Goldfarb, 1964).

If one depicts the stripping process as such that the residual nucleus of (A + 1) nucleons can be made up of the initial target of A nucleons coupled to the stripped neutron in a specific single particle orbit, the wave function of the final state may be expanded in terms of states arising from the vector coupling of the states of A target nucleons to the states of the stripped particle (Glendenning, 1963):

$$\psi_{J_f T_f}^{M_f}(A+1) = \sum_{l j J_c T_c} \beta_{lj}(J_c T_c ; J_f T_f) \sum_{M_c m_j M_{T_c}} \langle J_c M_c j m_j | J_f M_f \rangle \times \langle T_c M_{T_c} \tfrac{1}{2} \tfrac{1}{2} | T_f M_{T_f} \rangle \psi_{J_c T_c}^{M_c}(A)\, \psi_{nljt}. \qquad (2\text{-}32)$$

The coupling is subject to the restrictions that triangle inequalities exist among the spin quantum numbers $(1\ \tfrac{1}{2}\ \tfrac{1}{2})$, $(J_c\ j\ J_f)$, and $(T_c\ \tfrac{1}{2}\ T_f)$. The quantity β_{lj} is the overlap integral between $\psi_{J_f T_f}^{M_f}$ and the various wave functions $\psi_{J_c T_c}^{M_c}$ vector coupled to the single particle neutron wave functions ψ_{nljt}.

Although there is summation over numerous indices in the general expression of equation (2-32), in practice, there are often a smaller number of terms than it would seem at first glance. For instance, if J_f is 0,

j can have only one value, that is J_c. Also, j is limited by the maximum orbital angular momentum of the stripped neutron, so the number of values of J_c is limited. If the neutron is stripped into one single particle orbit only for a given transition, l is limited to one value, and j is limited to a maximum of two values. Hence, J_c has a maximum of two values.

Now consider the effect of substitution of equation 2-32 in the expression for the transition amplitude given in equation (2-18). The transition matrix for (d,p) becomes

$$T_{if} = \sum_{lj J_c T_c} \beta_{lj}(J_c T_c; J_f T_f) \sum_{M_c m_j M_{T_c}} \langle J_c M_c \, j \, m_j \,|\, J_f M_f \rangle \langle T_c M_{T_c} \tfrac{1}{2} \tfrac{1}{2} \,|\, T_f M_{T_f} \rangle$$
$$\times \langle \psi_p^{(-)}(\bar{k}_p, \bar{r}_p') \chi_{\nu_2}^{M_p} \gamma_{\nu_2}^{\nu_2} \psi_{J_c T_c}^{M_c}(A) \psi_{nljt} \,|\, V_{pn} + Q(V_{pA}) P \,|\, \psi_d^{(+)}(\bar{k}_d, \bar{R}) \Phi_d(\bar{r}) \chi_1^{M_d} \gamma_0^{\nu_d} \psi_{J_i T_i}^{M_i}(A) \rangle . \quad (2\text{-}33)$$

The first term of the potential does not operate on either $\psi_{J_i T_i}^{M_i}$ or $\psi_{J_f T_f}^{M_f}$, so these two functions may be conjugated out. The only non-vanishing term occurs when $J_c = J_i$, $T_c = T_i$, and $M_c = M_i$, that is, when the state of the core in the residual nucleus corresponds to the target ground state. This corresponds to the assumption that the core is undisturbed during the reaction. Since $\psi_{J_c T_c}^{M_c}$ is essentially a ground state wave function, the projection operator Q, then, causes the matrix to vanish when it is applied to $\psi_{J_c T_c}^{M_c}$. This is expected because the second term of T_{if} corresponds to core excitation. Since this possibility is small, in the simple pick-up or stripping formalism, the second term of the potential is ignored.

The perturbation, then, is considered to be due entirely to the proton - neutron interaction in the deuteron. Now, the transition amplitude can be more simply expressed.

$$T_{if} = \sum_{l j m_j} \beta_{lj} (J_i T_i j J_f T_f) \langle J_i M_i j m_j | J_f M_f \rangle \langle T_i M_{T_i} \tfrac{1}{2} \tfrac{1}{2} | T_f M_{T_f} \rangle \quad (2\text{-}34)$$
$$\times \langle \psi_p^{(-)}(\bar{k}_p, \bar{r}_p') \chi_{1/2}^{\mu_p} \tau_{1/2}^{\nu_p} \psi_{nljt} | V_{pn} | \psi_d^{(+)}(\bar{k}_d, \bar{R}) \varphi_d(\bar{r}) \chi_1^{\mu_d} \gamma_0^{\nu_d} \rangle$$

The bound neutron wave function can be further decomposed (Glendenning, 1963) to show explicitly the spin and orbital angular momentum coupling.

$$\psi_{nljt} = \sum_{m_l m_s} \langle l\ m_l\ \tfrac{1}{2}\ m_s | j m_j \rangle\ i^l\ \varphi_{nl}^{m_l}(\bar{r}_n)\ \chi_{1/2}^{m_s}\ \gamma_{1/2}^{1/2} \quad (2\text{-}35)$$
$$\varphi_{nl}^{m_l}(\bar{r}_n) = u_{nl}(r_n)\ Y_l^{m_l}(\theta_n)$$

The wave function $u_{nl}(r_n)$ is the radial part of the single particle wave function for the neutron bound in an orbital with n radial nodes and orbital angular momentum l. The potential must be central to get spherical harmonics, and the method of calculating $u_{nl}(r_n)$ will be discussed in chapter 3.

Substituting equations 2-29, 2-30, and 2-35 into 2-34, the transition amplitude becomes.

$$T_{if} = -\sum_{\substack{l m_l j m_j \\ m_s \mu_s \mu_p}} \frac{(-i)^l}{\sqrt{2}} \beta_{lj} (J_i T_i j J_f T_f) \langle J_i M_i j m_j | J_f M_f \rangle$$
$$\times \langle T_i M_{T_i} \tfrac{1}{2} \tfrac{1}{2} | T_f M_{T_f} \rangle \langle l\ m_l\ \tfrac{1}{2}\ m_s | j m_j \rangle \langle \tfrac{1}{2}\ \mu_p\ \tfrac{1}{2}\ \mu_s | 1 \mu_d \rangle$$
$$\times \langle \psi_p^{(-)}(\bar{k}_p, \bar{r}_p')\ u_{nl}(r_n)\ Y_l^{m_l}(\theta_n)\ \chi_{1/2}^{\mu_p}\ \chi_{1/2}^{m_s}\ \tau_{1/2}^{-1/2}(1)\ \tau_{1/2}^{1/2}(2) \ | V_{pn}$$
$$| \psi_d^{(+)}(\bar{k}_d, \bar{R})\ \varphi_d(\bar{r})\ \chi_{1/2}^{\mu_p}\ \chi_{1/2}^{m_s} [\tau_{1/2}^{-1/2}(1)\ \tau_{1/2}^{1/2}(2) - \tau_{1/2}^{1/2}(1)\ \tau_{1/2}^{-1/2}(2)] \rangle . \quad (2\text{-}36)$$

The factor $\frac{1}{\sqrt{2}}$ comes from the Clebsch - Gordon coefficient

for isospin in equation 2-30. Various simplifications are immediately apparent. For instance, the potential V_{pn} is assumed to be spin and isospin independent for this calculation, so the spin and isospin wave functions can be immediately conjugated out. A new quantity $B_l^{m_l}$ (Glendenning, 1963) is defined, and the transition amplitude may then be written as

$$T_{if} = \frac{-1}{\sqrt{2}} \sum_{\substack{l j m_j \\ m_l m_s}} \sqrt{2l+1}\, \beta_{lj} B_l^{m_l} \langle J_i M_i \; j m_j | J_f M_f \rangle \langle T_i M_{T_i} \tfrac{1}{2} \tfrac{1}{2} | T_f M_{T_f} \rangle \times \langle l m_l \tfrac{1}{2} m_s | j m_j \rangle \langle \tfrac{1}{2} \mu_p \tfrac{1}{2} m_s | 1 \mu_d \rangle , \tag{2-37}$$

$$B_l^{m_l} = \frac{(-i)^l}{\sqrt{2l+1}} \left\langle \psi_p^{(-)}(\bar{k}_p, \bar{r}_p') \, \varphi_{nl}^{m_l}(\bar{r}_n) \middle| V_{pn} \middle| \psi_p^{(+)}(\bar{k}_d, \bar{R}) \, \varphi_d(\bar{r}) \right\rangle . \tag{2-38}$$

To find the differential cross section, it is necessary to perform a rather tedious calculation of the square modulus of T_{if} summed over the initial and final spin orientations.

$$\sum_{\substack{M_i M_f \\ \mu_p \mu_d}} |T_{if}|^2 = \frac{\langle T_i M_{T_i} \tfrac{1}{2} \tfrac{1}{2} | T_f M_{T_f} \rangle^2}{2} \sum_{\substack{l l' \\ j j' \\ m_l m_l' m_j m_j' \\ M_i M_f \mu_p \mu_d m_s m_s'}} \sqrt{(2l'+1)(2l+1)}\, \beta_{l'j'}^{*} \beta_{lj} B^{*m_l'}_{l'} B^{m_l}_{l}$$
$$\times \langle J_f M_f | J_i M_i \; j' m_j' \rangle \langle J_i M_i \; j m_j | J_f M_f \rangle \langle j' m_j' | l' m_l' \tfrac{1}{2} m_s' \rangle$$
$$\times \langle l m_l \tfrac{1}{2} m_s | j m_j \rangle \langle \tfrac{1}{2} \mu_p \tfrac{1}{2} m_s | 1 \mu_d \rangle^2 \langle 1 \mu_d | \tfrac{1}{2} \mu_p \tfrac{1}{2} m_s' \rangle \tag{2-39}$$

The intermediate steps of this calculation appear in Appendix A. Substituting the result of appendix A into equation 2-22 and using $S_t = 1$ and $a = 2$ for the deuteron, the differential cross section for the (d,p) reaction is written as

$$\frac{d\sigma}{d\Omega} = \frac{1}{2}\frac{\mu_i\mu_f}{(2\pi\hbar^2)^2}\frac{k_f}{k_i}\frac{(2J_f+1)}{(2J_i+1)}\langle T_i M_{T_i} \tfrac{1}{2} \tfrac{1}{2} | T_f M_{T_f}\rangle^2$$

$$\times \sum_{l_j m_j} (A+1)|\beta_{lj}|^2 |B_l^{m_l}|^2. \qquad (2\text{-}40)$$

A quantity called the spectroscopic factor (Mac Farlane and French, 1960; Glendenning, 1963) is defined as

$$\mathcal{S}(l) = \sum_j \mathcal{S}(lj) = (A+1)|\beta_{lj}|^2. \qquad (2\text{-}41)$$

This quantity is further explored in the next section, but it should be noted that at this point the differential cross section has been reduced to the product of two factors, the first $\mathcal{S}(l)$ involves the spin geometry and the second $|B_l^{m_l}|^2$ involves the reaction dynamics. The next section is devoted to the calculation of spectroscopic factors in the shell model, and the third chapter explains the detailed numerical integration of $|B_l^{m_l}|^2$.

2.4 The Spectroscopic Factor in the Shell Model J T Representation

The spectroscopic factor is dependent on the overlap integral between the nuclear wave functions in the initial and final states. Hence, it depends on the nuclear model which generates the wave functions, and, for this reason, it can be used as a test of the validity of a specific model of a nucleus. The formalism has been treated in detail elsewhere (Mac Farlane and French, 1960),

so only the outlines will be given here.

In the previous section, $\beta_{\ell j}$ was introduced as an expansion coefficient of $\psi^{M_f}_{J_f T_f}(A+1)$ in terms of states arising from the vector coupling of $\psi^{M_c}_{J_c T_c}(A)$ to $\psi_{n\ell jt}$, the complete wave function of the bound neutron.

$$\beta_{\ell j} = \left\langle \psi^{M_f}_{J_f T_f}(A+1) \middle| \left[\psi^{M_c}_{J_c T_c}(A) \otimes \psi_{n\ell jt} \right]^{J_f T_f M_f} \right\rangle \qquad (2\text{-}42)$$

This is possible as long as $\psi^{M_c}_{J_c T_c}(A) \otimes \psi_{n\ell jt}$ forms a complete Hilbert space and is independent of the nuclear model used to generate the wave functions. In what follows, the overlap integral will be evaluated using shell model j-j coupling base functions. In this model a single particle orbit is designated by (n l j t) or simply (j). If there are n particles occupying the single particle orbit j, they are denoted by $(j)^n$. A system of particles occupying a set of single particle orbits is called a configuration.

To evaluate $\beta_{\ell j}$, it is convenient to use the technique of fractional parentage expansion. The technique is essentially a method for antisymmetrizing a system of n identical particles with reference to a set of base functions representing a system of n - m identical particles, where m<n. The relevance to stripping and pick-up reactions is apparent. Consider, for instance, a target nucleus whose ground state, $\psi^{M_i}_{J_i T_i}(n)$ is a member of the $(j)^n$ configuration. When a nucleon is stripped into the orbit j, the final state, $\psi^{M_f}_{J_f T_f}(n+1)$, is a member of the $(j)^{n+1}$ configuration. The antisymmetrized final state wave function

can then be expanded in terms of the vector coupling of single particle states, j, to the various possible $(j)^n$ configurations.

$$\psi^{M_f}_{J_f T_f}(n+1) = \sum_{J'T'} [(j)^n J'T', j, J_f T_f \,|\}\, (j)^{n+1} J_f T_f] \,|\, [\psi^{M'}_{J'T'} \otimes j]^{J_f T_f M_f} \rangle \qquad (2\text{-}43)$$

The quantity $[(j)^n J'T', j, J_f T_f \,|\}\, (j)^{n+1} J_f T_f]$ is called the coefficient of fractional parentage or cfp (de-Shalit and Talmi, chap. 33, 1963), and it has the following property:

$$\sum_{J'T'} [(j)^n J'T', j, J_f T_f \,|\}\, (j)^{n+1} J_f T_f]^2 = 1 . \qquad (2\text{-}44)$$

Substituting equation 2-43 into equation 2-42 and carrying out the integration, one finds, since the cfp is a real quantity (de-Shalit and Talmi, chap.33, 1963),

$$\beta_{lj} = [(j)^n J_i T_i, j, J_f T_f \,|\}\, (j)^{n+1} J_f T_f] . \qquad (2\text{-}45)$$

Reference to equation 2-41 immediately leads to a value for the spectroscopic factor.

$$S(lj) = (n+1)[(j)^n J_i T_i, j, J_f T_f \,|\, (j)^{n+1} J_f T_f]^2 \qquad (2\text{-}46)$$

Here, A has been replaced by n, the number of active nucleons participating in the reaction. The spectroscopic factor for the pick-up reaction is found by merely interchanging the subscripts i and f in equations 2-43 through 2-46. Equation 2-44 leads to the important sum rule (French and Mac Farlane, 1960).

$$\sum_{J_f T_f} S(lj) = n+1 \qquad (2\text{-}47)$$

Normally, the nuclear wave functions are more complicated than the simple $(j)^n$ configuration. For instance, a target nucleus ground state of the form $|(j_1)^{n_1} J_i T_i\ (j_2)^{n_2-1} J_2 T_2 ; J_i T_i\rangle$ may have a nucleon stripped into the j_2 orbital, which gives a final state $|(j_1)^{n_1} J_i T_i\ (j_2)^{n_2} J_f' T_f'; J_f T_f\rangle$. The overlap integral is given by French and Mac Farlane (1960) and Glendenning (1963).

$$\begin{aligned}\beta_{\ell j} = &\left[\frac{n_2}{n_1+n_2}\right]^{1/2}\left[(j_2)^{n_2-1} J_2 T_2, j_2, J'T' \,|\, (j_2)^{n_2} J'T'\right] \\ &\times\left[(2J'+1)(2J_i+1)(2T'+1)(2T_i+1)\right]^{1/2} W(j_2 J_2 J_f J_i; J' J_i) \\ &\times W(t_2 T_2 T_f T_i; T' T_i)\end{aligned} \tag{2-48}$$

Where W is the Racah coefficient (Brink and Satchler, 1968; Edmonds, 1960).

In the more general case, the nuclear states can be constructed as a linear combination of configurations (French and Mac Farlane, 1960).

$$\begin{aligned}\Psi^{M_i}_{J_i T_i}(n) &= \sum_\mu K_\mu \phi^\mu_{J_i T_i}(n) \\ \Psi^{M_f}_{J_f T_f}(n+1) &= \sum_\nu K_\nu \phi^\nu_{J_f T_f}(n+1),\end{aligned} \tag{2-49}$$

Where K are the amplitudes for each configuration. In this case, $\beta_{\ell j}$ is given by

$$\begin{aligned}\beta_{\ell j} &= \sum_{\mu\nu} K_\mu K_\nu \left\langle \phi^\nu_{J_f T_f}(n+1) \,\middle|\, \phi^\mu_{J_i T_i}(n) \otimes j \right\rangle \\ &= \sum_{\mu\nu} \beta^{\mu\nu}_{\ell j},\end{aligned} \tag{2-50}$$

and

$$S(\ell j) = (n+1)\,|\beta_{\ell j}|^2. \tag{2-51}$$

A closer examination of equation 2-48 leads to some helpful intuition concerning the construction of

nuclear states. For the ground state of light nuclei, closed orbitals are filled in such a way that both J_1 and T_1 are 0. This means that the spin and isospin of the ground state is determined by the configuration of the outermost nucleons. For n nucleons, and for a given set of available orbitals, it is possible, in some cases, that the spin-related quantum numbers of certain observed states of a nucleus could not be reproduced, especially if the active nucleons are restricted to those available in the outermost shell. In a more refined calculation, it might be possible to generate the proper spin-related quantum numbers, but, especially for high lying states, it might not be possible to reproduce the excitation energy. The nucleons in the inner orbitals are more tightly bound than those in the outermost; and, hence they require more energy to remove them from their orbitals. So it is most probable that these nucleons are actively involved in the construction of highly excited states. Construction of these states, then, involves the core excitation which was ruled out where $Q(V_{pc})P$ was deleted from the matrix element in equation 2-33. The assumption can be restated in terms of the characteristics of wave functions: For low-lying states of the residual nucleus, the components of the wave function corresponding to core excitation have neglegible amplitudes. On the other hand, in highly excited states, where core excitation amplitudes are not neglegible, the reaction theory, as here formulated is inadequate.

When both J_1 and T_1 are 0, the spectroscopic

factor takes an especially simple form.

$$\mathcal{S}(lj) = n_2 \left[(j_1)^{n_1-1} J_1 T_1, j_2 J' T' \right\} (j_1)^{n_2} J' T' \Big]^2 \qquad (2\text{-}52)$$

It is important to note that there are no quantities in this expression which refer to the closed orbitals. For the purposes of the calculation, in the approximation that there are no core excitations, the only effect of the inner nucleons is in the kinematic part.

At the beginning of this section, it was stated that the spectroscopic factor can be used to test nuclear models. It should now be clear how this is done. The spectroscopic factor is sensitive to the different components which can be added to the initial state wave function. The amplitudes can be arrived at, for instance, by fitting the states with the amplitudes as parameters. The same sort of thing can be done for the final state wave function. However, it is possible that a specific wave function could fit the nuclear states, but predict spectroscopic factors of entirely the wrong magnitude. If this were the case, it would be an indication of a breakdown in the model. Alternatively, agreement between experimental and theoretical spectroscopic factor is a partial confirmation of the model.

For the work carried out here, only light nuclei whose outer nucleons occupy the 1_p shell are dealt with. The cfp's for these nuclei have been computed by several authors; in L-S coupling by Jahn and van Wieringen (1950 and 1951) and by Mac Farlane and French (1960), and in j-j coupling by Flowers (1952) and Edmonds and Flowers (1952).

The spectroscopic factors extracted in this work will be compared with those calculated by Cohen and Kurath (1967).

CHAPTER 3

METHODS OF NUMERICAL COMPUTATION

3.1 The Radial Integral

From the definition given in equation 2-38, the reaction dynamics factor, which contains the angular distribution in the transition amplitude can be written explicitly in the form

$$B_l^{m_l} = \frac{(-i)^l}{\sqrt{2l+1}} \int d\bar{r}_n \, d\bar{r}_p \, \psi_p^{(-)*}(\bar{k}_p, \bar{r}_p') \, Y_l^{m_l *}(\hat{r}_n) \, u_{n,l}^*(r_n) \times V_{pn}(\bar{r}) \, \varphi_d(\bar{r}) \, \psi_d^{(+)}(\bar{k}_d, \bar{R}) . \qquad (3\text{-}1)$$

This is a six dimensional integral which must be simplified before it can be evaluated.

From the geometry of the reaction (Figure 1) and relations 2-23 through 2-26, it is possible to make the following substitutions.

$$\bar{R} = \bar{r}_n + \gamma \bar{r} \qquad (3\text{-}2)$$

$$\bar{r}_p' = \lambda \bar{r}_n + \bar{r} \qquad (3\text{-}3)$$

where $\gamma = m_p / m_d$ and $\lambda = M_A / M_{A+1}$. Here, the subscripted masses refer to the proton (p), deuteron (d), target (A), and residual nucleus (A + 1). With the substitutions of equations 3-2, 3-3 and transforming the variables $\bar{r}_p$ and $\bar{r}_n$ to $\bar{r}_n$ and $\bar{r}$, an intermediate integral is defined, which will be used for some of the simplifications in later sections of this chapter

$$I(\bar{r}_n) = \int d\bar{r} \, \psi_p^{(-)*}(\bar{k}_p, \bar{r} + \lambda \bar{r}_n) \, V_{pn}(\bar{r}) \, \varphi_d(\bar{r}) \, \psi_d^{(+)}(\bar{k}_d, \gamma \bar{r} + \bar{r}_n), \qquad (3\text{-}4)$$

and

$$B_l^{m_l} = \frac{(-i)^l}{\sqrt{2l+1}} \int d\bar{r}_n \, I(\bar{r}_n) \, Y_l^{m_l *}(\hat{r}_n) \, u_{n,l}^*(r_n). \qquad (3\text{-}5)$$

Two common approximations often used in evaluating equation 3-4 are the zero range approximation and the finite range approximation. Both of these will be discussed in this chapter. First, though, it is necessary to discuss the method of generating the distorted waves, $\psi_p^{(-)*}$ and $\psi_d^{(+)}$, and the radial part of the bound neutron wave function u_{nl}^*.

3.2 The Distorted Waves

The distorted waves, $\psi_p^{(-)*}$ and $\psi_d^{(+)}$, are assumed to be generated by a Schrödinger equation similar to equations 2-14 and 2-15, with optical potentials V_p and V_d, respectively. It is further assumed that the optical potentials are central, so the distorted waves $\psi_p^{(-)*}$ and $\psi_d^{(+)}$ can be expanded in terms of the spherical harmonics (Bassel et al., 1962).

$$\psi_p^{(-)*}(\bar{k}_p, \lambda \bar{r}_n) = \frac{4\pi}{k_p \lambda r_n} \sum_{L_p M_p} Y_{L_p}^{M_p *}(\hat{r}_n)\, Y_{L_p}^{M_p}(\hat{k}_p)\, i^{-L_p}\, \psi_{L_p}(k_p \lambda r_n) \qquad (3\text{-}6)$$

$$\psi_d^{(+)}(\bar{k}_d, \bar{r}_n) = \frac{4\pi}{k_d r_n} \sum_{L_d M_d} Y_{L_d}^{M_d *}(\hat{r}_n)\, Y_{L_d}^{M_d}(\hat{k}_p)\, i^{L_d}\, \psi_{L_d}(k_d r_n) \qquad (3\text{-}7)$$

Note that the distorted waves are expanded in terms of $\bar{r}_n$ only and not $\bar{r}$. This is possible since in both approximations used to evaluate equation 3-5 the integration over $\bar{r}$ is performed first, and the distorted waves will not be introduced in expanded form until this is done.

In either the incident or outgoing channel,

the Schrödinger equation used to generate the distorted waves can be written as follows:

$$\left[\frac{d^2}{dr^2} + k_i^2 = \frac{2\mu_i}{\hbar^2} V_c - \frac{2\mu_i}{\hbar^2} V_{op} - \frac{L(L+1)}{r^2}\right] \Psi_L(k_i r) = 0 \qquad (3\text{-}8)$$

where V_c, V_{op} and μ_i are the Coulomb potential, optical potential, and the reduced mass, respectively. The Coulomb potential is assumed to be that for a point source up to a specified distance ,R_c, from the origin. Inside that distance, the charge distribution is assumed to be isotropic and the potential function is given by (Houdayer, 1969)

$$\begin{aligned} V_c &= \frac{Z_1 Z_2 e^2}{r} \qquad r > R_c \\ &= \frac{3 Z_1 Z e^2}{2 R_c}\left[1 - r^2/3R_c^2\right] \qquad r < R_c . \end{aligned} \qquad (3\text{-}9)$$

The potential V_{op} is an optical potential of the form (Houdayer, 1969),

$$\begin{aligned} V_{op} = V_o F_o(r) &= \left(\frac{\hbar}{m_\pi c}\right)^2 V_{so} \frac{1}{r}\frac{d}{dr} F_{so}(r) \langle \vec{l}\cdot\vec{s} \rangle \\ &+ i\left\{ W_V F_V(r) - 4 a_D W_D \frac{d}{dr} F_D(r) \right\}, \end{aligned} \qquad (3\text{-}10)$$

where

$$F_x(r) = \frac{1}{1 + e^{(r-R_x)/a_x}} , \qquad (3\text{-}11)$$

which is the Woods-Saxon form factor. The quantity R_x is a measure of the potential well radius, and is taken to be $R_x = r_x A^{1/3}$, where A is the nuclear mass number, and a_x is the diffuseness parameter, which determines the slope of the potential well. For small a_x the slope approaches infinity, that is, a square well, and as a_x approaches infinity, the slope becomes 0. For intermediate

values of a_x, the well shape is similar to that of the harmonic oscillator well. The four terms given in equation 3-10 are the real potential (V_o), the spin-orbit potential (V_{so}), and the imaginary volume (W_v) and imaginary surface (W_d) potentials. The four quantities in parentheses are the well depth parameters for each of the potentials. For the deuteron channel, the spin-orbit term is set equal to zero. The effect of this assumption will be discussed later.

The nuclear potential is short-ranged, so the asymptotic form of the radial part of the distorted waves is similar to the Coulomb wave function (Abramowitz and Stegun, 1965; Bassel et al., 1962),

$$\psi_L(k_i r) \rightarrow e^{i\sigma_L}\left[F_L(k_i r) + C_L H_L(k_i r)\right]$$
$$\sim \frac{1}{2i}\left[e^{-i(k_i r - \eta_i \ln 2k_i r - L\pi/2)} - e^{2i(K_L+\sigma_L)} e^{i(k_i r - \eta_i \ln 2k_i r + L\pi/2)}\right] \quad (3\text{-}12)$$

The constant σ_L and C_L contain, respectively, the Coulomb and nuclear potential phase shifts, $\sigma_L = \arg\Gamma(1+L+i\eta_i)$, and $C_L = e^{iK_L}\sin K_L$, where K_L is the nuclear phase shift. The Coulomb parameter, $\eta_i = z_1 z_2 e^2 \mu_i / \hbar^2 k_i$. H_L is a linear combination of the regular (F_L) and irregular (G_L) Coulomb wave functions, $H_L = G_L + iF_L$. If both the Coulomb and nuclear potentials are 0, the Coulomb wave functions reduce to the spherical Bessel and Hankel functions, and when these are substituted into equation 3-6 or 3-7, the expansions become the standard ones for plane waves. This, of course, confirms that the distorted wave approximation

converges to the plane wave approximation in the limit of small distorting potentials.

In order to generate the wave functions numerically, the following approximation is used (Smith, 1965; Milne, 1962):

$$\frac{\Psi_L(r+\delta)-2\Psi_L(r)+\Psi_L(r-\delta)}{\delta^2} \simeq \frac{\Psi_L''(r+\delta)+10\Psi_L''(r)+\Psi_L''(r-\delta)}{12} \quad (3\text{-}13)$$

This leads to the iteration formula

$$\Psi_L(r+\delta)=\frac{\left[12-10g(r)\right]\Psi_L(r)-g(r-\delta)\Psi_L(r-\delta)}{g(r+\delta)}, \quad (3\text{-}14)$$

where δ is the increment in r and

$$g(r) = 1-\frac{\delta^2}{12}\frac{\Psi_L''(r)}{\Psi_L(r)}. \quad (3\text{-}15)$$

The boundary conditions are that $\Psi_L(0)=0$, and that at a sufficiently large value of r, $\Psi_L(r)$ matches the asymptotic value of the Coulomb wave function given in equation 3-12. In fact, the calculation is performed by generating $\Psi_L(r)$ starting from the origin and normalizing to the value of the Coulomb wave function at two adjacent points at large r.

3.3 The Bound State Neutron Wave Function

The radial neutron wave function $u_{n\ell}(r_n)$ is generated using the Schrödinger equation

$$\left[\frac{d^2}{dr_n^2}+k^2-\frac{2\mu}{\hbar^2}V(r_n)-\frac{\ell(\ell+1)}{r_n^2}\right]u_{n\ell}(r_n)=0, \quad (3\text{-}16)$$

where the potential $V(r_n)$ is of the same form as the one given in equation 3-10, except that there is no imaginary term. Since there is no Coulomb potential, and since the

neutron is bound, the asymptotic form of $u_{n\ell}(r_n)$ is given by letting σ and η go to 0 in equation 3-12, and by letting k go to ik (Smith, 1965).

$$u_{n\ell}(r_n) \longrightarrow \frac{1}{2i} e^{i(2K_\ell + \ell\pi/2)} e^{-kr} \tag{3-17}$$

The wave function is generated numerically starting from the asymptotic value and going toward the origin using the numerical differentiation approximation

$$u''_{n\ell}(r) \simeq \frac{u_{n\ell}(r+\delta) - 2u_{n\ell}(r) + u_{n\ell}(r-\delta)}{\delta^2}. \tag{3-18}$$

The spin-orbit potential parameters are held fixed, but the real well depth is varied so the wave function meets the boundary condition at the origin.

3.4 The Zero-Range Approximation

The zero-range approximation is the mathematical expression of the assumption that the transition matrix element is negligible except when the neutron and proton coordinates of the deuteron coincide. The assumption is expressed by replacing the product of $V_{pn}(\bar{r})\,\varphi_d(\bar{r})$ in equation 3-4 by $g\delta(\bar{r})$, where

$$g = \int d\bar{r}'\, V_{pn}(\bar{r}')\,\varphi_d(\bar{r}') \tag{3-19}$$

is a constant correction factor, which is the zero-momentum component of the Fourier transform of $V_{pn}(\bar{r})\,\varphi_d(\bar{r})$. If the spin-dependence of the proton-neutron interaction is ignored, and only the s-wave part of the deuteron wave function is considered, the Hulthén wave function (equation-2-31) and Hulthén potential can be used in the integral

of equation 3-19 (Buttle and Goldfarb, 1964).

$$V_{pn} = -\frac{\hbar^2}{\mu}(\beta^2-\alpha^2)\frac{e^{-\beta r}}{e^{-\alpha r}-e^{-\beta r}}, \tag{3-20}$$

where

$$\alpha = \left(\frac{\mu B_d}{\hbar^2}\right)^{1/2}; \quad \beta \simeq 7\alpha . \tag{3-21}$$

In equations 3-20 and 3-21, μ is the reduced mass of the deuteron, and B_d is the deuteron binding energy.

When the integration of equation 3-4 is performed, the intermediate integral, $I(\bar{r}_n)$, takes the form

$$I(\bar{r}_n) = g\,\psi_p^{(-)*}(\bar{k}_p, \lambda\bar{r}_n)\,\psi_d^{(+)}(\bar{k}_d, \bar{r}_n). \tag{3-22}$$

When $I(\bar{r}_n)$ is introduced into equation 3-5 and the expansions in spherical harmonics given in equations 3-6 and 3-7 are employed, the angular parts of the integration can be performed leaving only a radial integral

$$B_\ell^{m_d} = \frac{g\sqrt{4\pi}}{k_p k_d \delta}\sum_{L_p L_d} i^{L_d-L_p-\ell}(2L_d+1)\langle L_d\, m_\ell\, \ell\, -m_\ell | L_p\, 0\rangle$$
$$\times \langle L_d\, 0\, \ell\, 0 | L_p\, 0\rangle \sqrt{\frac{(L_d-m_\ell)!}{(L_d+m_\ell)!}}\, P_{L_d}^{m_\ell}(0) \int d\bar{r}_n\, \psi_{L_p}^{(-)*}(k_p\lambda r_n)\, u_{n\ell}^*(r_n)\, \psi_{L_d}^{(+)}(k_d r_n). \tag{3-23}$$

The integral can be evaluated numerically using the trapezoidal rule (Smith, 1965; Milne, 1962).

$$\int dr_n\, \psi_{L_p}^{(-)*}(k_p\lambda r_n)\, u_{n\ell}^*(r_n)\, \psi_{L_d}^{(+)}(k_d r_n) \tag{3-24}$$
$$= \epsilon \sum_{j=1}^{N} \psi_{L_p}^{(-)*}(\lambda j\epsilon)\, u_{n\ell}^*(j\epsilon)\, \psi_{L_d}^{(+)}(j\epsilon)$$

where ϵ is the increment.

The effect of the zero-range approximation is to make the incident and outgoing particle coordinate vectors parallel, that is $\bar{r}_p' = \lambda\bar{r}_n$. In some cases, the zero-range theory tends to overestimate the differential cross sections. This problem is thought (Li, 1967) to be

due to a tendency for the theory to overestimate the contribution to the integral from inside the residual nucleus. To correct for this, an approximation called the finite-range approximation is introduced. The effect of this is to reduce the overall magnitude of the cross-section, while retaining much of the simplicity of the zero-range approximation.

3.5 The Finite-Range Approximation

In equation 3-19, it is noted that g is the zero-momentum component of the Fourier transform of $V_{pn}(\bar{r})\,\varphi_d(\bar{r})$. For the zero-range approximation, $V_{pn}(\bar{r})\,\varphi_d(\bar{r})$ is assumed to be sharply peaked at $\bar{r}=0$, so the δ-function is employed. The Fourier transform of the δ-function is a constant, and similarly, g is a constant. If one were to assume that the sharpness of the peak was less than that warranted by the δ-function approximation, the Fourier transform of $V_{pn}(\bar{r})\,\varphi_d(\bar{r})$ would not be given by a constant. However, for small distances from $\bar{r}=0$, it would be safe to assume the Fourier transform is a slowly varying function of momentum.

In equation 3-4, it is possible to expand the distorted waves in a Taylor series about $\bar{r}=0$, since $V_{pn}(\bar{r})\,\varphi_d(\bar{r})$ is a short range function, and there is no need to know the properties of the distorted waves for large $\bar{r}$. The Taylor expansion leaves $I(\bar{r}_n)$ in the form

$$I(\bar{r}_n)=\int d\bar{r}\; V_{pn}(\bar{r})\,\varphi_d(\bar{r})\,e^{i\bar{K}\cdot\bar{r}}\,\psi_p^{(-)*}(\bar{k}_p,\lambda\bar{r}_n)\,\psi_d^{(+)}(\bar{k}_d,\bar{r}_n). \qquad (3\text{-}25)$$

The integral can be evaluated by noting that $\bar{K}$ is independent of $\bar{r}$ (Buttle and Goldfarb, 1964). This, then, is the Fourier transform of $V_{pn}(r)\,\varphi_d(r)$, and should be a smoothly varying function of $\bar{K}$. Using this property, the integral is evaluated by Buttle and Goldfarb (1964) and Li (1967). The result is

$$I(\bar{r}_n) = -\left(\frac{\alpha+\beta}{\beta}\right)^{3/2} \frac{\hbar^2 (8\pi\alpha)^{1/2}}{\mu} \frac{\beta^2}{\beta^2 + K_1^2} \psi_p^{(-)*}(\bar{k}_p, \lambda\bar{r}_n)\,\psi_d^{(+)}(\bar{k}_d, \bar{r}_n). \quad (3\text{-}26)$$

The operator K_1^2 is defined as

$$K_1^2 = \left(\gamma^2 - \frac{\gamma}{\lambda}\right) K_d^2 + (1 - \gamma\lambda) K_p^2 + \frac{\gamma}{\lambda} K_n^2, \quad (3\text{-}27)$$

where K_n^2, K_p^2, and K_d^2 are defined by the Schrodinger equations

$$\left\{ K_n^2 - \frac{2\mu}{\hbar^2}(B_d + V_{nc}(\bar{r}_n)) \right\} \psi_{nlj,t}(r_n) = 0, \quad (3\text{-}28)$$

$$\left\{ K_p^2 - \frac{2\mu_f}{\hbar^2}(V_f(\bar{r}_n) - E_p) \right\} \psi_p^{(-)*}(\bar{k}_p, \lambda\bar{r}_n) = 0, \quad (3\text{-}29)$$

and

$$\left\{ K_d^2 - \frac{2\mu_i}{\hbar^2}(V_i(\bar{r}_n) - E_d) \right\} \psi_d^{(+)}(\bar{k}_d, \bar{r}_n) = 0. \quad (3\text{-}30)$$

In equations 3-28, 3-29, and 3-30, $V_{nc}(\bar{r}_n)$ is the potential for the bound neutron, and $V_i(\bar{r}_n)$ and $V_f(\bar{r}_n)$ are, respectively, the optical potentials for generating the distorted waves in the incident and outgoing channels.

The distorted waves can be expanded as they were in section 3.4, and the same angular integral can be performed. If $\bar{g}(K_1)$ is defined

$$\bar{g}(K_1) = -\left(\frac{\alpha+\beta}{\beta}\right)^{3/2} \frac{\hbar^2 (8\pi\alpha)^{1/2}}{\mu} \frac{\beta^2}{\beta^2 + K_1^2}, \quad (3\text{-}32)$$

the matrix element can be written

$$B_\ell^{m_\ell} = \frac{\sqrt{4\pi}}{k_p k_d \delta} \sum_{L_p L_d} i^{L_d - L_p - \ell} (2L_d+1) \langle L_d\, m_\ell\, \ell - m_\ell \mid L_p\, 0 \rangle$$

$$\times \langle L_d\, 0\, \ell\, 0 \mid L_p\, 0 \rangle \sqrt{\frac{(L_d - m_\ell)!}{(L_d + m_\ell)!}}\, P_{L_d}^{m_\ell}(\theta) \int dr_n\, \bar{g}(K_1)\, \psi_{L_p}^{(-)*}(k_p \lambda r_n)\, u_{n\ell}^*(r_n)\, \psi_{L_d}^{(+)}(k_d r_n). \qquad (3\text{-}33)$$

The remaining task is to evaluate the radial integral using the method mentioned at the end of section 3.4.

CHAPTER 4

ANALYSIS OF THE REACTION $^{9}Be(p,d)\ ^{8}Be$

4.1 Method of Analysis

The experimental data to be analyzed are the $^{9}Be(p,d)\ ^{8}Be$ reaction obtained at proton energies of 46 MeV (Verba et al., 1967) and 100 MeV (Mark, 1965; Lee et al., 1967). These data are reproduced for convenience in tables 4-1 and 4-2. Comparing the (p,d) data with the partial energy level scheme of ^{8}Be in figure 2 (Lauritsen and Ajzenberg-Selove, 1966), it is evident that some comment is necessary. Verba et al. observed six deuteron groups corresponding to the states listed in table 4-1. The experiment was done with an energy resolution of ± .1MeV. In addition, they observed a small group at 11.4 MeV and another at 24.5 MeV. Kull (1967) has done the same experiment at 33.6 MeV, and his observations agree for the most part with Verba's. They both find that the 16.63 MeV state is excited only about 5% compared to the 16.93 MeV state. However, the state which Verba identifies as 19.05 MeV, Kull identifies as 19.22 MeV. Neither author mentions any contribution from the broad 18.9 MeV state which appears in the energy level diagram. For the purpose of this analysis, Verba's designation of the 19MeV deuteron group as resulting from the excitation of the 19.05 MeV state in ^{8}Be will be assumed. The data from Lee et al. using 100 MeV protons were taken with energy resolution of 1.9 MeV. The

TABLE 4-1

Differential cross sections from ^{9}Be (p,d) ^{8}Be at 46 MeV.[a]

Ground state		2.90 MeV state		16.93 MeV state	
θ_{cm} (deg.)	$d\sigma/d\Omega_{cm}$ (mb/sr)	θ_{cm} (deg.)	$d\sigma/d\Omega_{cm}$ (mb/sr)	θ_{cm} (deg.)	$d\sigma/d\Omega_{cm}$ (mb/sr)
15.0	3.55	15.3	7.07	15.8	4.77
17.3	2.76	17.6	4.93	18.3	4.53
20.3	2.13	20.6	4.28	21.3	3.73
23.2	1.58	23.5	3.28	24.3	2.73
29.0	.82	29.3	2.49	30.3	1.52
34.8	.54	35.1	2.08	36.3	1.23
40.5	.335	40.8	1.65	42.2	1.27
46.7	.205	46.5	1.32	48.1	1.12
52.0	.116	52.2	.867	53.9	.787
57.5	.062	57.8	.473	59.7	.459
63.5	.067	63.3	.392	65.3	.310
69.0	.048	68.8	.264	70.9	.284
74.0	.035	74.2	.230	76.5	.269
79.5	.037	79.6	.168	81.9	.272
84.5	.040	84.8	.125	87.2	.238
90.0	.02	90.0	.137	92.5	.162
100.0	.0082	100.2	.0670	102.6	.104
105.0	.0047	105.1	.0390	107.6	.0937
110.0	.0046	110.0	.0261	112.4	.0722
119.5	.0057	119.5	.0272	117.2	.0564
124.0	.0067	128.8	.0260	126.4	.0768
129.5	.0061	137.8	.0250	135.3	.0573
133.5	.0041			139.6	.0547
138.0	.0087				

a) Verba et al., 1967.

TABLE 4-1 (CONT.)

17.64 MeV state		18.15 MeV state		19.05 MeV state	
θ_{cm} (deg.)	$d\sigma/d\Omega_{cm}$ (mb/sr)	θ_{cm} (deg.)	$d\sigma/d\Omega_{cm}$ (mb/sr)	θ_{cm} (deg.)	$d\sigma/d\Omega_{cm}$ (mb/sr)
12.0	.97	16.0	.84	12.3	1.64
15.0	1.10	18.3	.37	15.4	1.55
15.6	.86	21.5	.175	16.0	1.35
18.0	1.13	24.5	.250	18.4	1.46
21.2	.61	30.5	.098	21.5	1.27
24.1	.51	36.5	.098	24.5	1.15
30.2	.263	42.5	.108	30.6	.683
36.0	.242	48.2	.102	36.6	.657
42.0	.207	54.1	.046	42.6	.572
48.0	.207	59.9	.0324	48.5	.585
53.9	.148	65.5	.0350	54.4	.440
59.7	.114	71.3	.0180	60.2	.307
65.2	.087	76.5	.0243	71.5	.196
71.0	.059	82.3	.0280	82.5	.167
76.1	.061	87.2	.0211	93.1	.118
82.0	.060	92.5	.0132	103.3	.0876
86.5	.055	103.0	.0086		
92.6	.044	108.0	.0161		
102.5	.0230	112.7	.0110		
107.1	.0229	117.5	.0150		
112.0	.0180	127.0	.0106		
116.5	.0170	135.5	.0091		
126.5	.0202	140.0	.0124		
135.1	.1254				
139.2	.0176				

TABLE 4-2

Differential cross sections from ^{9}Be (p,d) ^{8}Be at 100 MeV.[a]

Ground state		2.90 MeV state		16-20 Mev states	
θ_{cm} (deg.)	$d\sigma/d\Omega_{cm}$ (mb/sr)	θ_{cm} (deg.)	$d\sigma/d\Omega_{cm}$ (mb/sr)	θ_{cm} (deg.)	$d\sigma/d\Omega_{cm}$ (mb/sr)
5.8115	1.6203	5.8249	3.0097	5.8992	6.3117
9.338	1.1164	9.3595	2.266	9.4787	5.7574
13.9859	.5411	14.0191	1.3341	14.197	3.9262
18.6727	.2272	18.7155	.8320	18.952	2.4438
23.3451	.1389	23.3982	.5556	23.6922	1.589
30.0893	.1079	30.1571	.3123	30.5322	.9723
34.9356	.07023	35.0237	.2256	35.4552	.5719
41.4923	.0391	41.5836	.1384	42.0882	.2489
45.2564	.02799	45.3549	.08933	45.8998	.1555
50.5804	.01661	50.6887	.0536	51.2879	.1008
57.5307	.01083	57.6509	.02919	58.3157	.07896
63.0699	.006107	63.1986	.01896	63.9109	.04607
69.9585	.004303	70.0906	.01166	70.8609	.02612
74.2766	.003145	74.4198	.008797	75.2124	.01875
85.1845	.001530	85.3375	.004111	86.1847	.003608

a) Mark, 1965; Lee et al., 1967

FIGURE 2

A partial diagram of the known energy levels of ^{8}Be. See Lauritsen and Ajzenberg-Selove (1966) for the complete diagram.

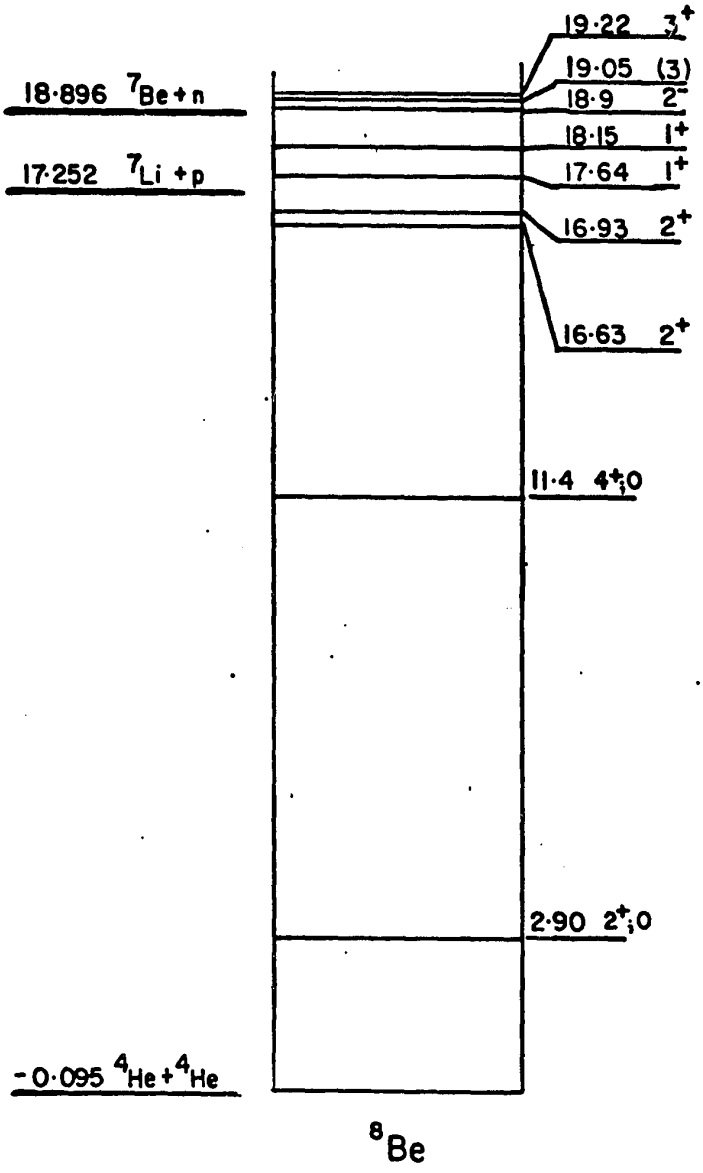
19·22 3+
19·05 (3)
18·9 2−
18·896 7Be+n
18·15 1+
17·252 7Li+p
17·64 1+
16·93 2+
16·63 2+
11·4 4+;0
2·90 2+;0
-0·095 4He+4He
8Be

deuteron group labeled 16-20 MeV presumably contains contributions from many levels of ^{8}Be in that energy region. For the purpose of this analysis it has been assumed that the major components are due to the 16.93, 17.64, 18.15, and 19.05 MeV states as observed by Verba and Kull.

In this analysis the transferred neutron was assumed initially to be bound in a Saxon-Woods potential of the form of equation 3-10 (with the imaginary part set equal to 0) in the target nucleus. The bound state of the neutron must be such that when it is coupled to the final state in the residual nucleus the initial state of the target is reproduced. The neutron potential well parameters used are given in table 4-3. The potential depth V_o has been adjusted to give the correct neutron binding energy with respect to the ground state of the residual nucleus.

The easiest method for obtaining the incoming and outgoing distorted waves would be to use the optical potential derived from fitting the elastic scattering data of protons from ^{9}Be and of deuterons from ^{8}Be. However, deuteron data were not available since ^{8}Be is unstable. Hence, a more complicated method has been adopted to obtain the deuteron optical potential. First, the proton potential is obtained by fitting the elastic scattering data, as mentioned above. Then, using this proton potential, the deuteron potential is generated by

TABLE 4-3

Neutron potential parameters.[a]

$r_o=r_{so}$	$a_o=a_{so}$	V_o	V_{so}
1.36	0.55	31.79	9.0

a) Li and Mark, 1969a

fitting the experimental angular distribution for the ground state transition in the $^{9}Be(p,d)\,^{8}Be$ reaction. Once the optical potential is found, analysis for the excited state transitions may be carried out with all parameters fixed.

Both the optical model and the DWBA computer codes were written by Dr. T.Y. Li in this laboratory. The entire calculation was performed using the IBM 360/75 computer in the McGill Computing Center. Details for operating the optical model code can be found in the thesis of Houdayer (1969) and for the DWBA code in appendix B of this work. The search subroutine used in both codes has been explained by Houdayer.

The automatic search subroutine operates by minimizing the quantity χ^2, which is defined as

$$\chi^2 = \sum_{i=1}^{N} \left| \frac{\sigma^{exp}(\theta_i) - \sigma^{theo}(\theta_i)}{\Delta\sigma(\theta_i)} \right|^2 , \qquad (4\text{-}1)$$

where $\sigma^{exp}(\theta_i)$ and $\sigma^{theo}(\theta_i)$ are, respectively, the observed and the calculated differential cross sections at center-of-mass angle θ_i, and $\Delta\sigma(\theta_i)$ is the error quoted for the data point. Since the optical potential is known to be ambiguous in the sense that several different potentials can give an adequate fit to the data, the absorption cross section, σ_R, is calculated in the optical model code. The aim is to compare the calculated value to the observed value as an additional criterion to distinguish the best potential.

At each energy, two sets of proton optical parameters

were found using the potential given in equation 3-10. In one set, the imaginary term had $W_V=0$, and in the other $W_D=0$. These parameter sets are called, respectively, the surface imaginary and the volume imaginary sets. In all cases, the Coulomb potential radius parameter, R_C, was 1.89 fm, the value quoted by Li and Mark (1968).

Table 4-4 shows the proton optical potential parameters found to give the best fit to the data. The 100 MeV sets were found by Li and Mark (1968). For the 46 MeV data, essentially the same search procedure was followed as for the 100 MeV data. In the latter case, however, the search was initiated using the 100 MeV parameters. First, the potential depths were varied with all the geometrical parameters fixed. Then, individually the restrictions on the geometrical parameters were relaxed until a minimum value for χ^2 was reached with nine parameters being varied. Figure 3 shows the two theoretical fits to the 46 MeV elastic scattering data.

Satchler (1967) has also analyzed the 46 MeV elastic scattering data using an optical model code. He observed that when the geometrical parameters in the imaginary potential were varied independently of those in the real potential, the radius parameter of the former tended to become larger than the one in the latter. A similar phenomenon was observed in potential P1, but not as strikingly as those given by Satchler. As a check on the optical parameters, they were used to calculate the

TABLE 4-4

Proton channel optical parameters from ^{9}Be (p,p) ^{9}Be.

Potential	Energy (MeV)	r_o (fm)	a_o (fm)	V_o (MeV)	r' (fm)	a' (fm)	W_V (MeV)	W_D (MeV)
P1	46	1.150	.74	34.74	1.31	.79	13.72	
P2	46	1.145	.76	42.41	.82	.64		17.09
P3	100[a]	1.457	.69	15.70	1.34	.51	13.41	
P4	100[a]	1.356	.67	16.77	1.38	.56		5.43

Potential	r_{so} (fm)	a_{so} (fm)	V_{so} (MeV)	σ_A calc (mb)	σ_A expt (mb)	χ^2/N
P1	1.052	.553	10.63	449	<490[b]	2.8
P2	1.024	.429	6.14	429	<490[b]	4.7
P3	1.035	.394	6.76	243	231	1.6
P4	1.294	.452	7.05	259	231	1.5

a) Li and Mark, 1968
b) Carlson et al., 1967

FIGURE 3

Optical model fitting of the 46 MeV elastic scattering data. The solid curve is potential P1, and the dashed curve is potential P2.

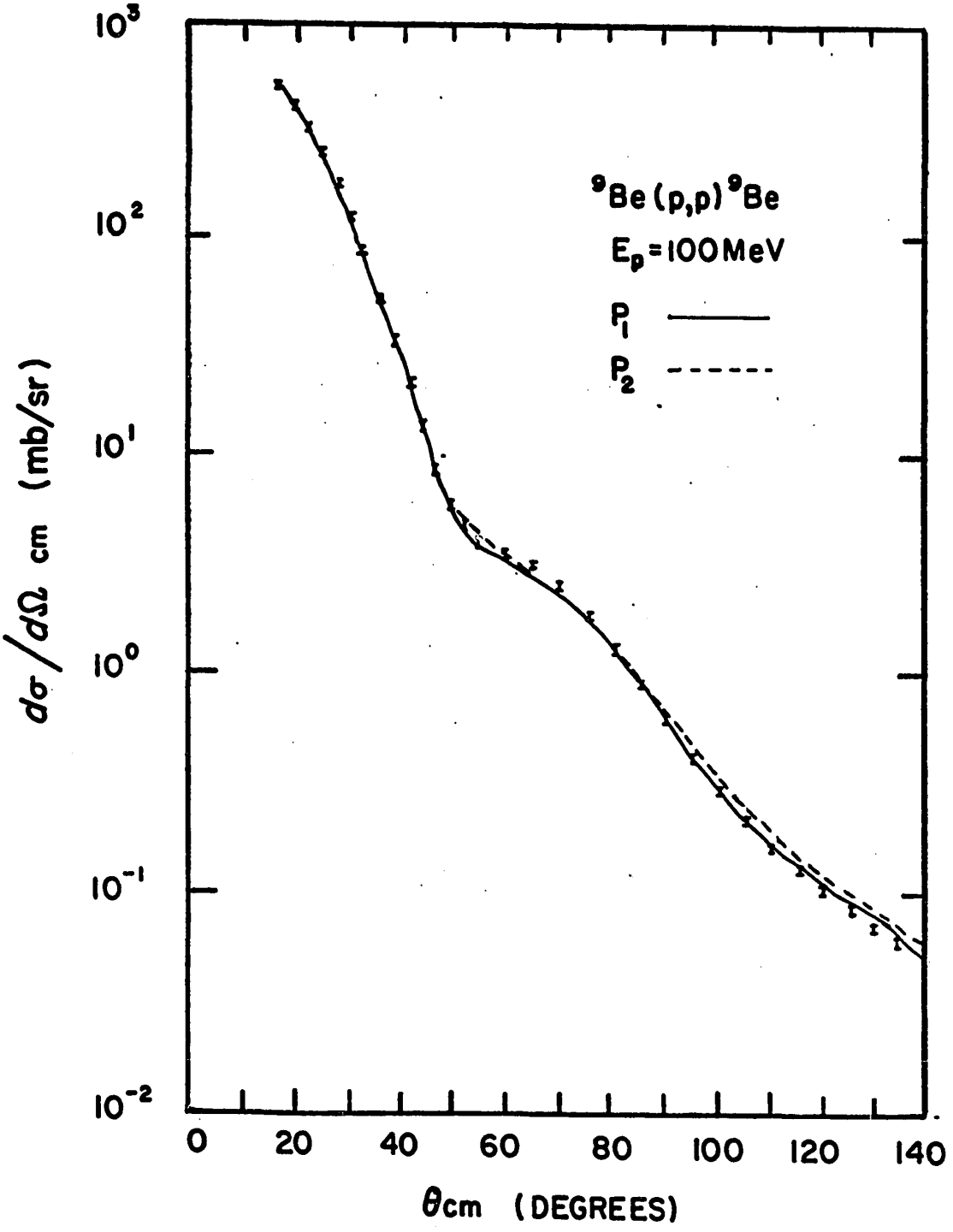
^{9}Be (p,p) ^{9}Be
E_p = 100 MeV
P_1
P_2
$d\sigma/d\Omega$ cm (mb/sr)
10^3
10^2
10^1
10^0
10^{-1}
10^{-2}
0
20
40
60
80
100
120
140
θcm (DEGREES)

42 MeV proton polarization data from ^{9}Be.

The fit was poor, which has also been noted by Satchler. This peculiar behavior of the optical model fitting of ^{9}Be might reflect something particular in the structure of ^{9}Be (Li and Mark 1968).

4.2 Results and Comparison With The Experiments

For each set of proton parameters, a deuteron surface imaginary parameter set was found using the DWBA code with the finite-range approximation. For this calculation, the spin-orbit coupling potential was assumed to be 0 in both channels. The (p,d) ground state transition angular distribution was fitted by supplying a theoretical value for the spectroscopic factor (Cohen and Kurath, 1967) in order to obtain order-of-magnitude agreement with experiment. The resulting calculated value is then normalized to the observed differential cross section.

The ^{9}Be ground state with spin and parity $J^{\pi} = 3/2^{-}$ was assumed to be prinicpally of the shell model configuration $(1s)^{4}(1p)^{5}$ and the pick-up process is expected to take place in the 1p shell. For this calculation it was assumed that only the l=1 nucleons were affected in the (p,d) reaction. This leads to the possibility of $j = 1 \pm \frac{1}{2} = \frac{1}{2}$ or 3/2 for the total angular momentum of the picked-up neutron. For the transition to the ground state (0^{+}) of ^{8}Be, only $j = 3/2$ is allowed.

The calculated angular distribution for the

ground state transition at 46 MeV incident energy with the two different combinations of proton and deuteron optical potentials appears in figures 4 and 5. Analysis of the same transition at 100 MeV incident energy gave the fittings shown in figures 6 and 7. Generally, the fits to the ground state are fairly good, and at each energy, they are similar to each other apart from a small difference in absolute normalization. In each case, the calculated curve has been normalized to the experimental points, and the root-mean-square deviation from the mean normalization has been calculated. The mean normalization and its deviation were used to extract the spectroscopic factors, which will be discussed in the next section.

The deuteron optical potentials obtained from the ground state transition at 46 MeV and 100 MeV incident energy are given in table 4-5. The Coulomb radius was taken to be $R_C = 1.4$ fm. Although the deuteron parameters at each energy show a certain amount of internal consistency, there seems to be some variability between the sets. At 100 MeV r_o is significantly smaller than that at 46 MeV. Also, while r_D and a_D are about the same size at 46 MeV, r_D is definitely larger than a_D at 100 MeV.

To analyze the excited states' transitions, the deuteron optical potentials extracted from the ground state transition were used. In every case except the 19.05 MeV state (3^+), the contributions from both $j = \frac{1}{2}$ and 3/2 pick-up were expected; for the 19.05 MeV state, only

FIGURE 4

Angular distribution for the ground state transition, showing the fit obtained using potential $46W_V$.

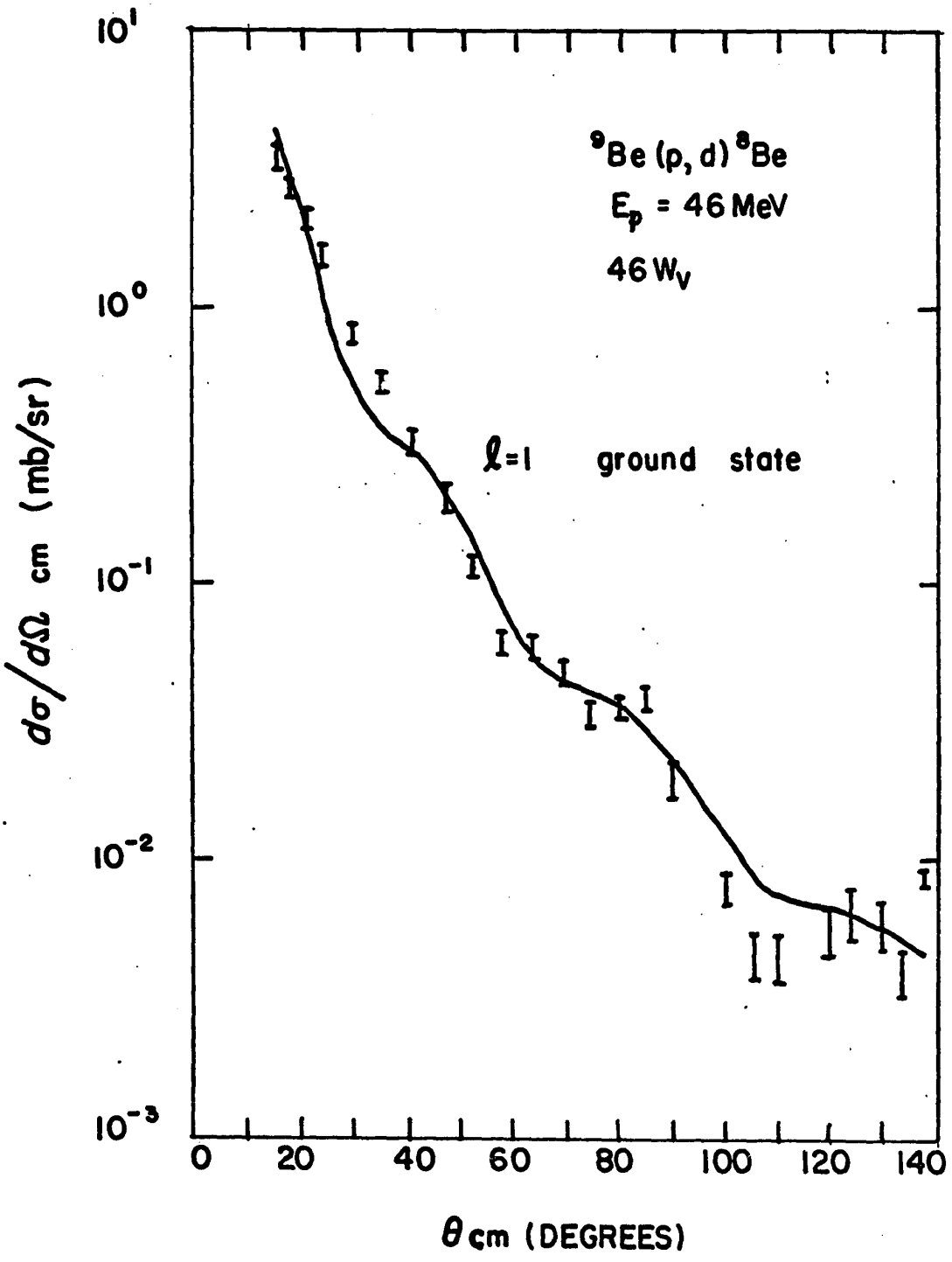
^{9}Be (p, d) ^{8}Be
E_p = 46 MeV
46 W_V
ℓ=1 ground state
$d\sigma/d\Omega$ cm (mb/sr)
θ cm (DEGREES)
10^1
10^0
10^{-1}
10^{-2}
10^{-3}
0
20
40
60
80
100
120
140

FIGURE 5

Angular distribution for the ground state transition, showing the fit obtained using potential $46W_D$.

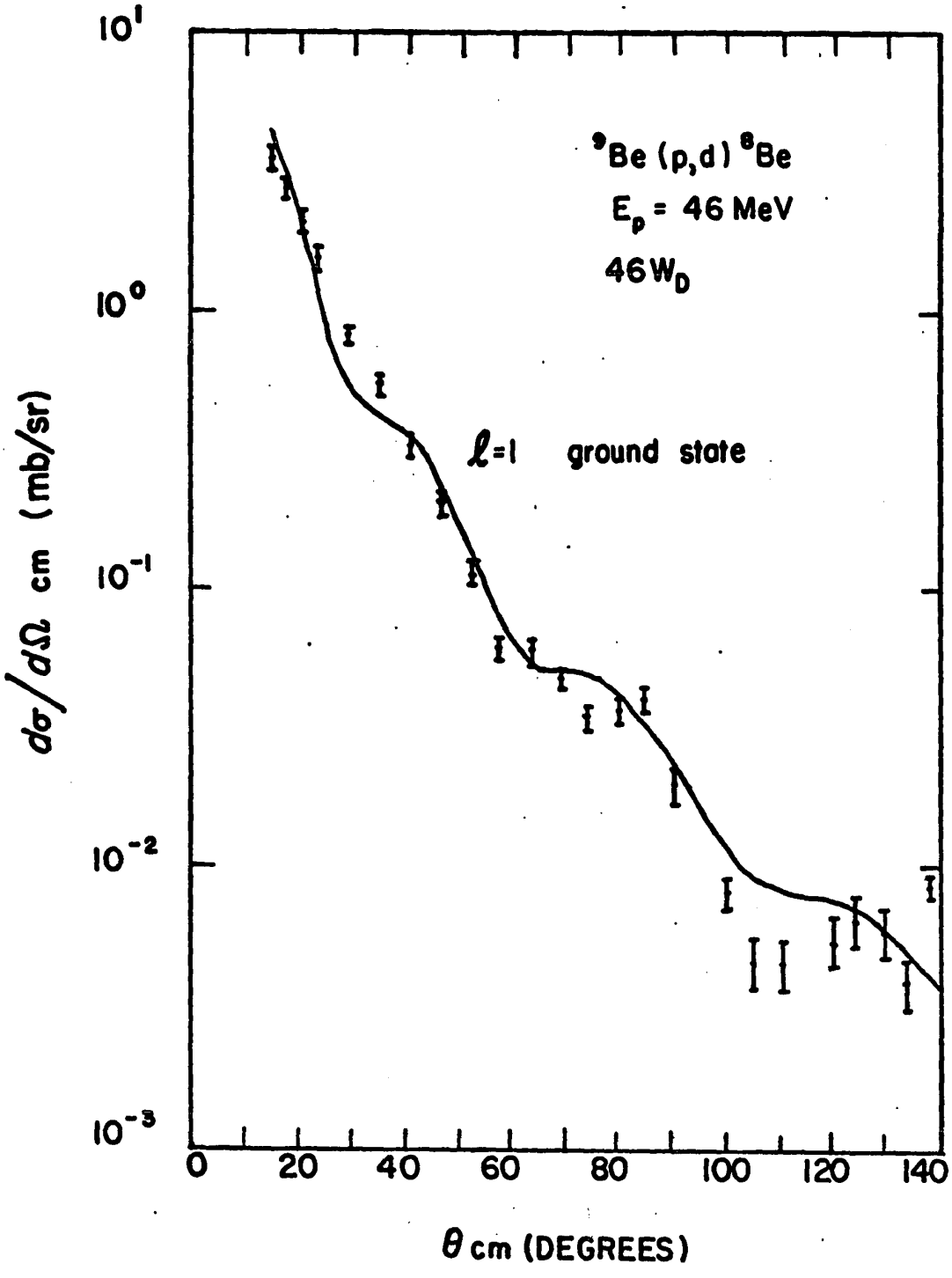
^{9}Be (p,d) ^{8}Be
E_p = 46 MeV
46 W_D
ℓ=1 ground state
$d\sigma/d\Omega$ cm (mb/sr)
θ cm (DEGREES)
10^1
10^0
10^{-1}
10^{-2}
10^{-3}
0
20
40
60
80
100
120
140

FIGURE 6

Angular distribution for the ground state transition, showing the fit obtained using potential $100W_V$.

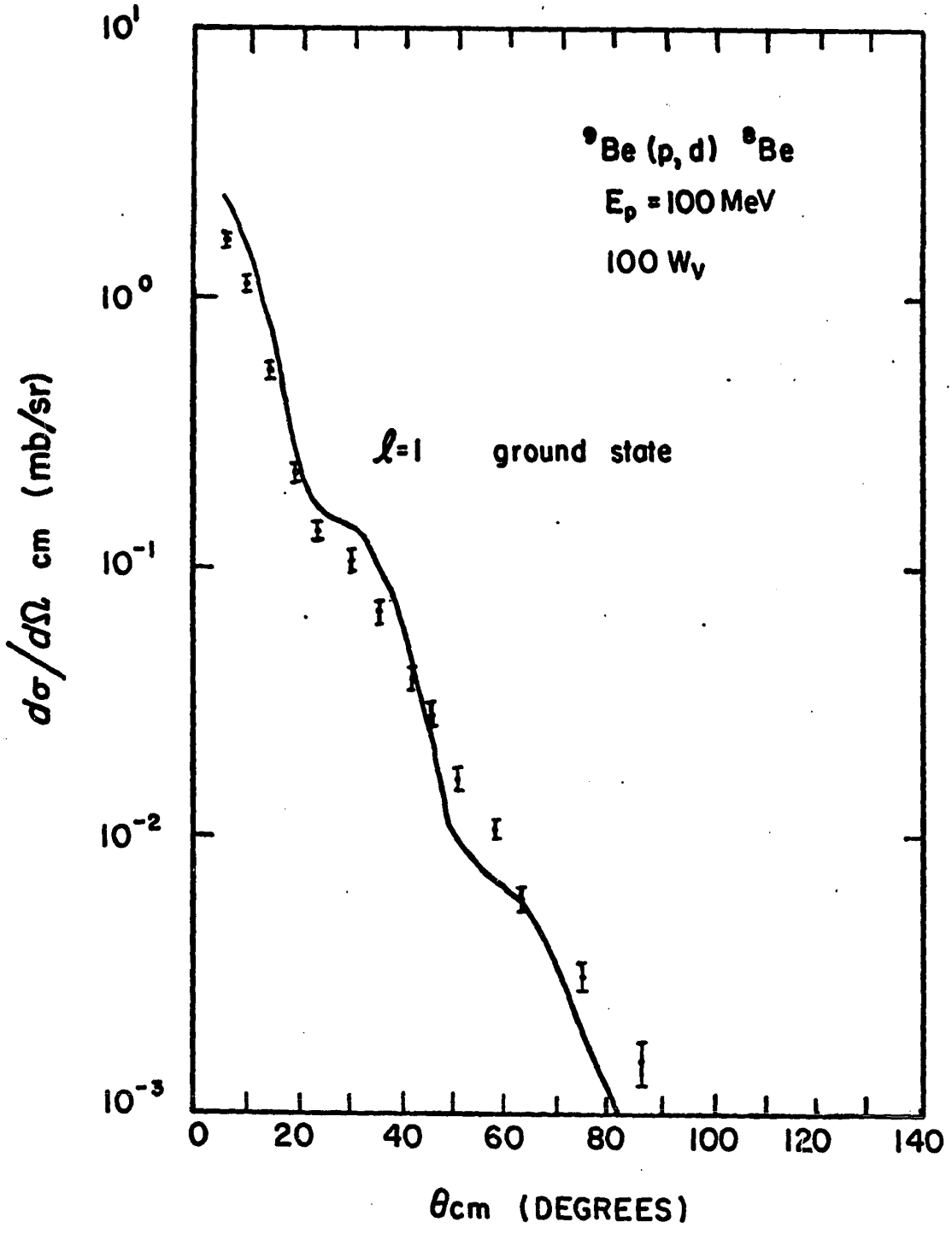
^{9}Be (p, d) ^{8}Be
E_p = 100 MeV
100 W_V
ℓ=1 ground state
$d\sigma/d\Omega$ cm (mb/sr)
10^1
10^0
10^{-1}
10^{-2}
10^{-3}
0
20
40
60
80
100
120
140
θcm (DEGREES)

FIGURE 7

Angular distribution for the ground state transition, showing the fit obtained using potential $100W_D$.

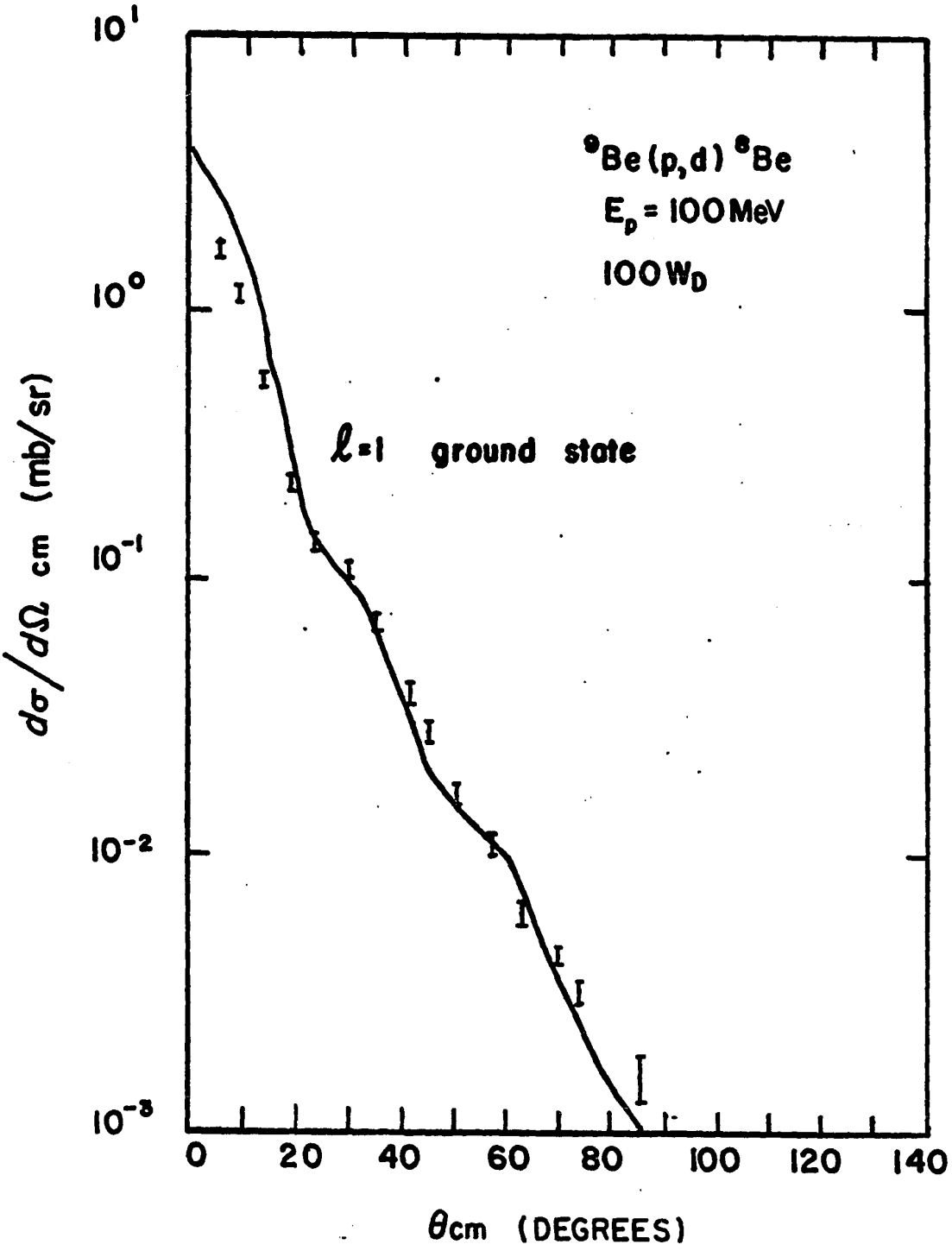
^{9}Be(p,d)^{8}Be
E_p = 100 MeV
100 W_D
ℓ=1 ground state
$d\sigma/d\Omega$ cm (mb/sr)
10^1
10^0
10^{-1}
10^{-2}
10^{-3}
0
20
40
60
80
100
120
140
θcm (DEGREES)

TABLE 4-5

Deuteron channel optical parameters from ^{9}Be (p,d) ^{8}Be.

Deuteron Potential	Proton Potential	Energy (MeV)	r_0 (fm)	a_0 (fm)	V_0 (MeV)
$46W_V$	P1	46	1.212	.45	72.63
$46W_D$	P2	46	1.176	.54	86.79
$100W_V$	P3	100	.614	.31	50.90
$100W_D$	P4	100	.849	.22	51.15

Deuteron Potential	r_D (fm)	a_D (fm)	W_D (MeV)	χ^2/N
$46W_V$	1.146	1.20	11.22	6.3
$46W_D$	.977	.99	14.63	5.2
$100W_V$	1.66	.85	18.30	15.9
$100W_D$	1.65	.87	18.03	11.9

$j = 3/2$ was allowed. To analyze transitions to the excited states in which both $j = \frac{1}{2}$ and $3/2$ are allowed, the theoretical relative spectroscopic factors as given by Cohen and Kurath (1967) have been used. The differential cross sections for a given transition were calculated separately for $j = \frac{1}{2}$ and $3/2$ components, and then, the sum of the two components, weighted by the relative spectroscopic factors for $j = \frac{1}{2}$ and $3/2$ pick-up, was normalized to the experimental data. The angular distributions for the excited states are given in figures 8 through 21.

For the 100 MeV data, the observed deuteron group in the excitation energy region from 16 to 20 MeV has been assumed to result mainly from the excitation of the four states (16.93, 17.64, 18.15, and 19.05 MeV) as observed by Verba at 46 MeV. The calculated angular distributions for this group of deuterons were obtained by simply adding the contributions from the four states mentioned above using the theoretical spectroscopic factors given by Cohen and Kurath. The fits in both cases (figures 20 and 21) were surprisingly good considering the complexity of the experimental data.

Comparison of the figures 4 through 21, shows that for a given pair of potentials, the calculated angular distributions are quite similar in shape. However, the magnitudes before normalization are somewhat different. These differences fall within the root-mean-square deviations,

FIGURE 8

Angular distribution for the 2.9 MeV state transition, showing the fit obtained using potential $46W_V$.

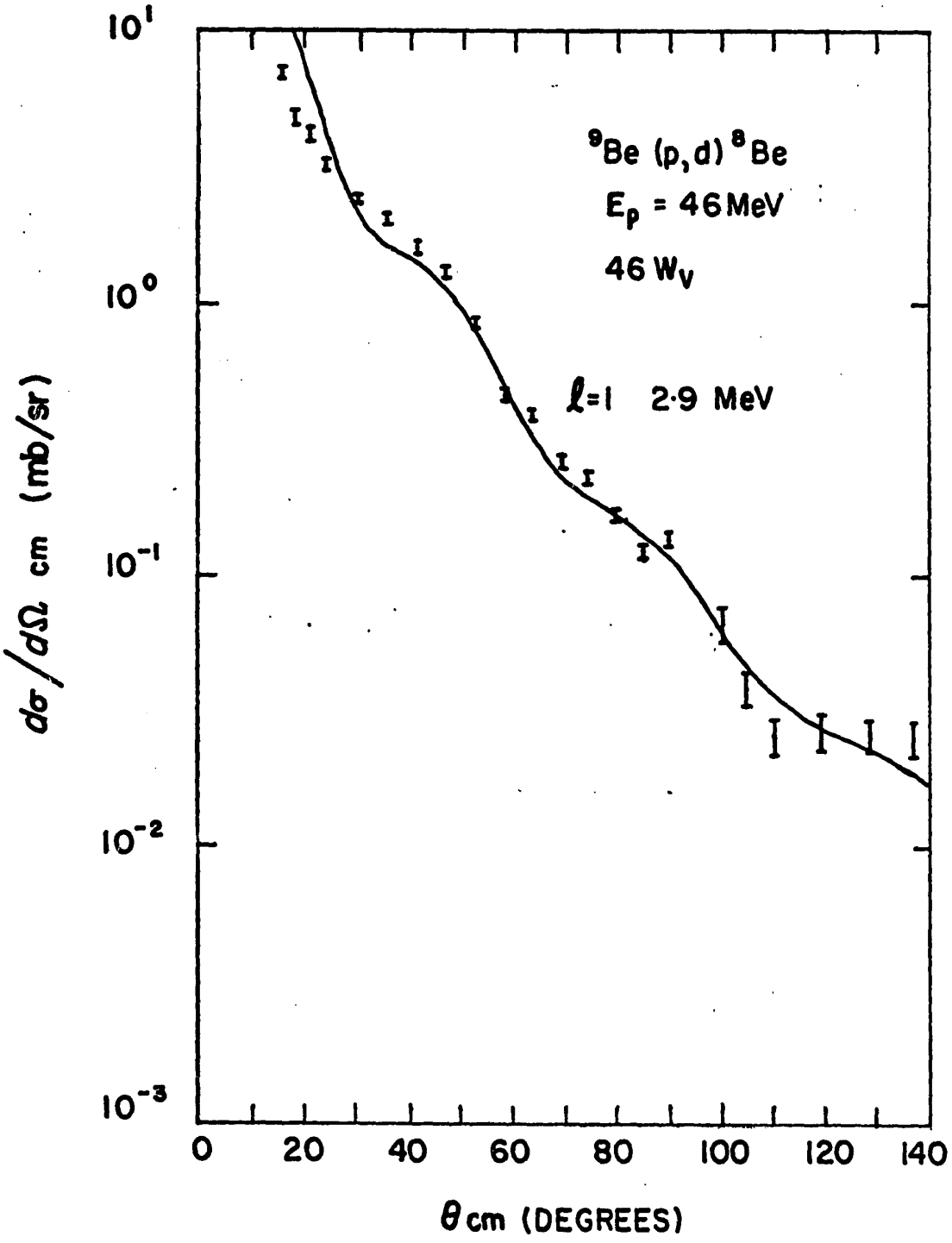
^{9}Be (p,d) ^{8}Be
E_p = 46 MeV
46 W_V
ℓ=1 2·9 MeV
$d\sigma/d\Omega$ cm (mb/sr)
θcm (DEGREES)
10^1
10^0
10^{-1}
10^{-2}
10^{-3}
0
20
40
60
80
100
120
140

FIGURE 9

Angular distribution for the 2.9 MeV state transition, showing the fit obtained using potential $46W_D$.

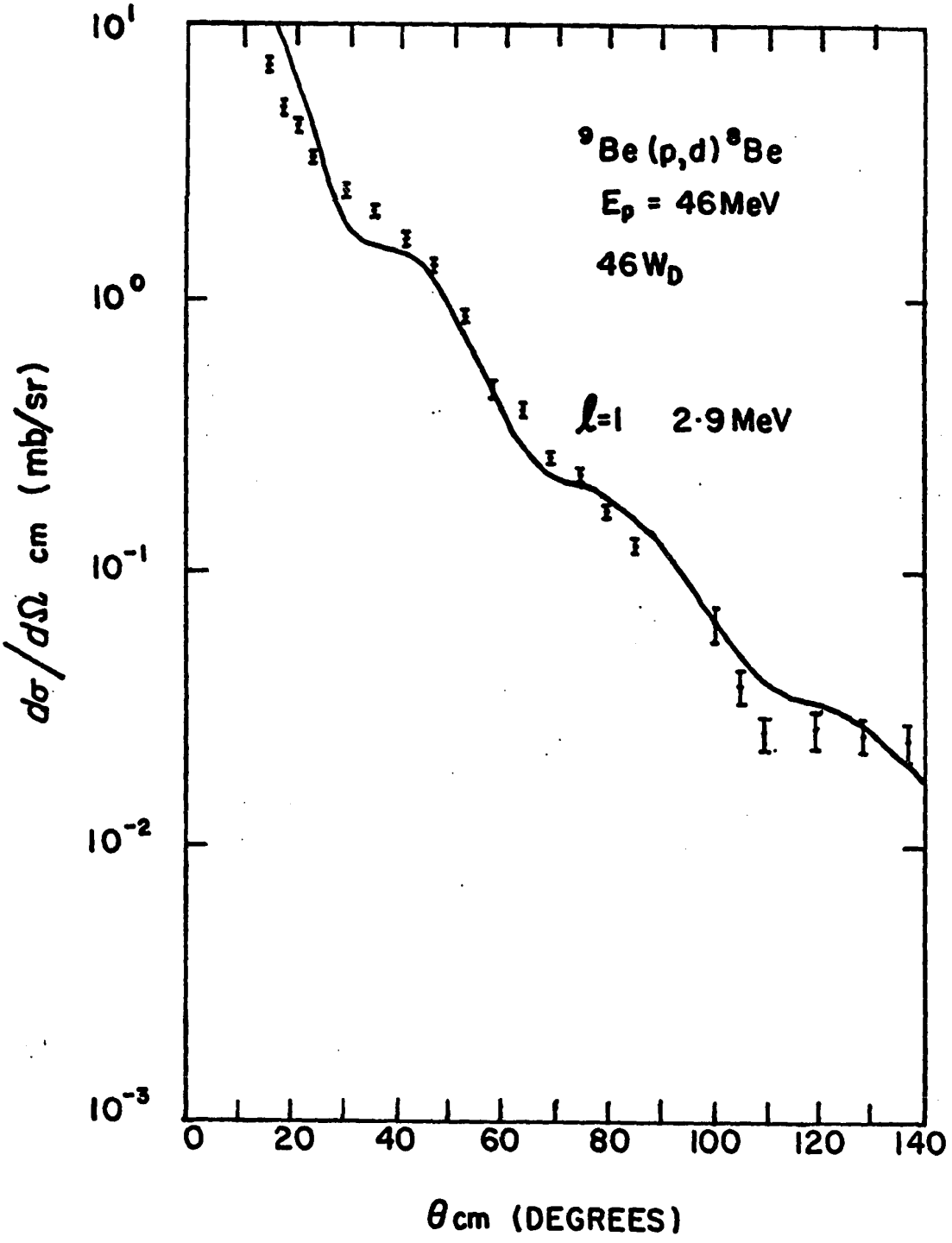
^{9}Be (p,d) ^{8}Be
E_p = 46MeV
46 W_D
ℓ=1 2·9MeV
$d\sigma/d\Omega$ cm (mb/sr)
θcm (DEGREES)
10^{1}
10^{0}
10^{-1}
10^{-2}
10^{-3}
0
20
40
60
80
100
120
140

FIGURE 10

Angular distribution for the 16.93 MeV state transition, showing the fit obtained using potential $46W_V$.

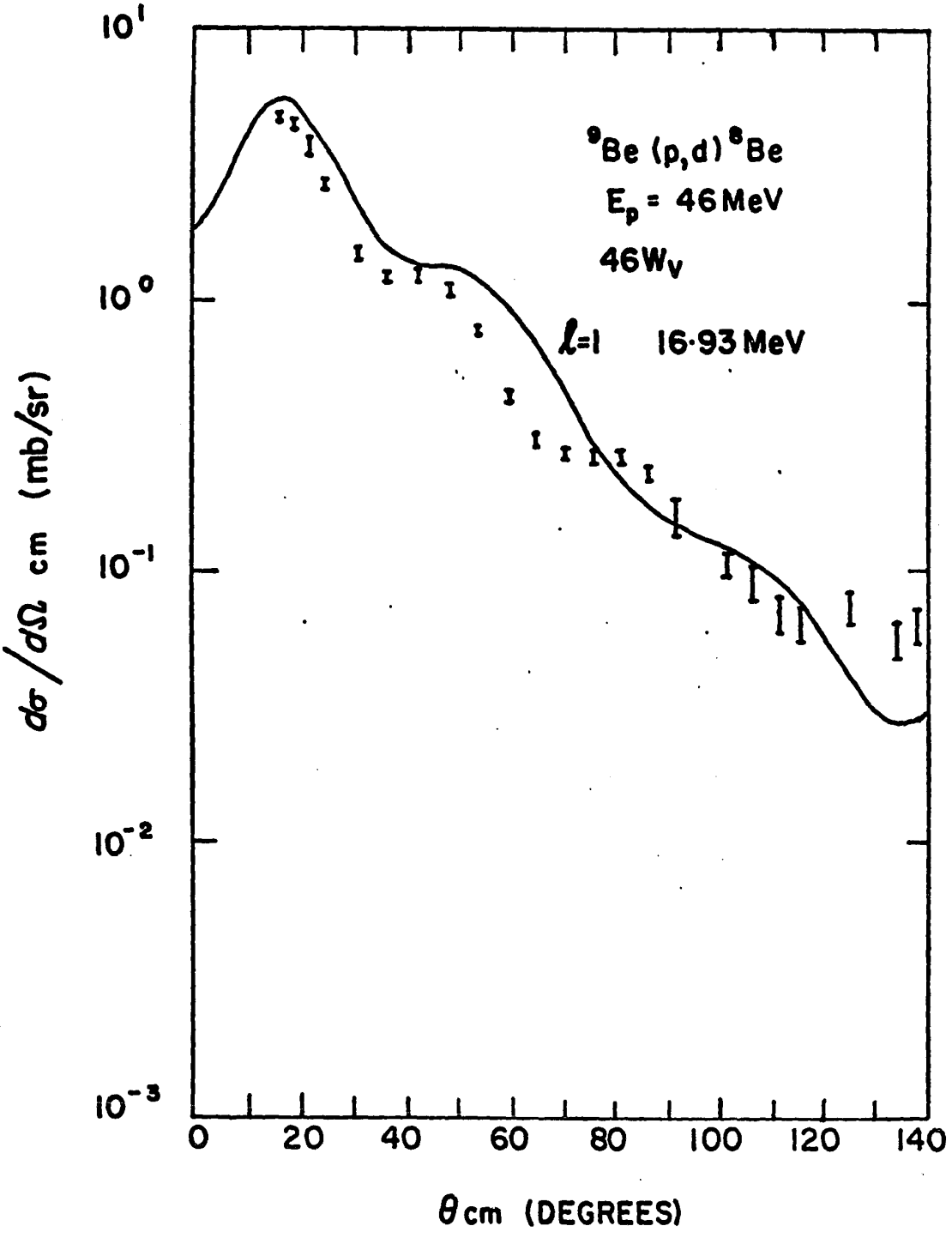
^{9}Be (p,d) ^{8}Be
E_p = 46 MeV
46 W_V
ℓ=1 16·93 MeV
$d\sigma/d\Omega$ cm (mb/sr)
θ cm (DEGREES)
10^{1}
10^{0}
10^{-1}
10^{-2}
10^{-3}
0
20
40
60
80
100
120
140

FIGURE 11

Angular distribution for the 16.93 MeV state transition, showing the fit obtained using potential $46W_D$.

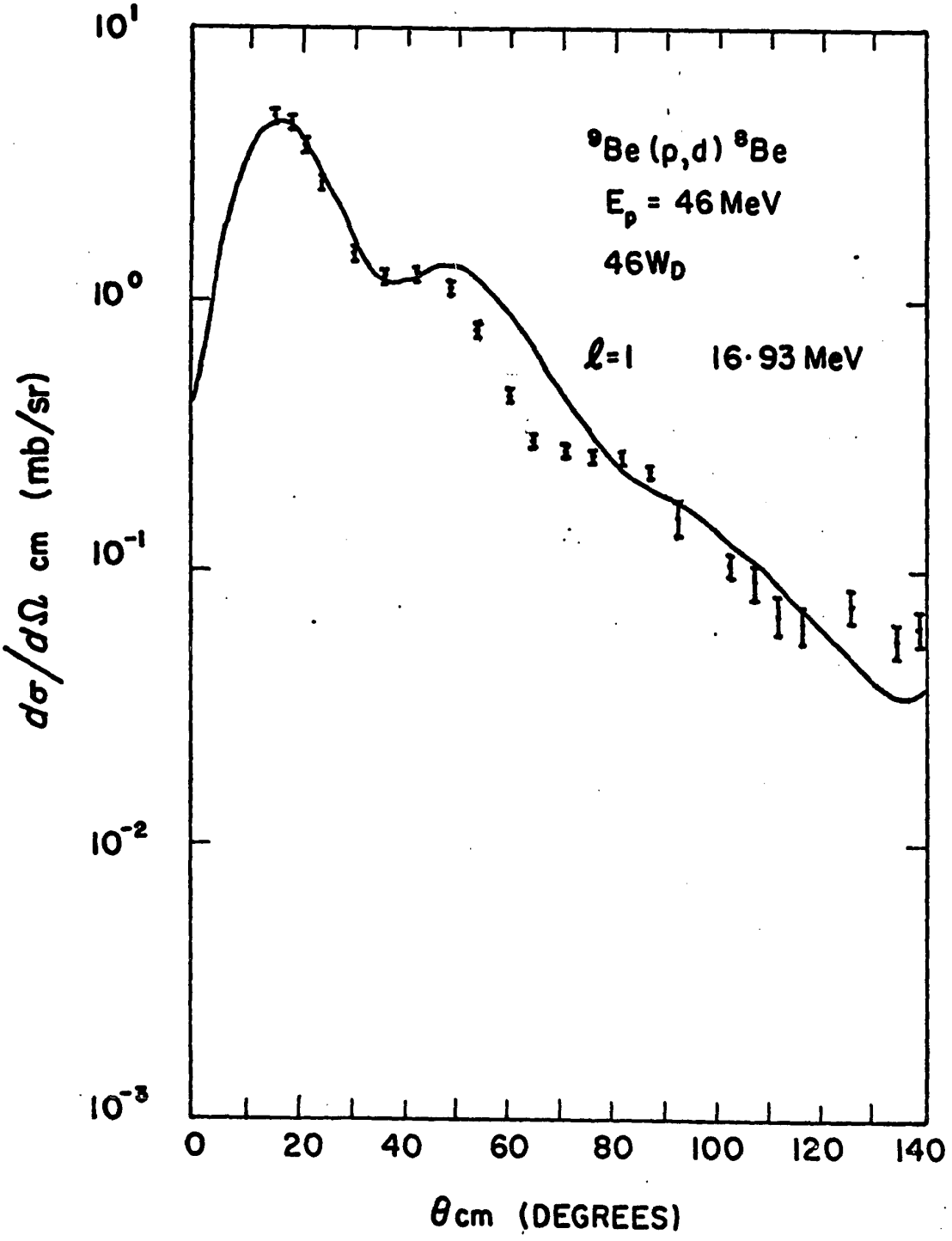
10^1
10^0
10^{-1}
10^{-2}
10^{-3}
$d\sigma/d\Omega$ cm (mb/sr)
^{9}Be (p,d) ^{8}Be
E_p = 46 MeV
46W$_D$
ℓ=1
16·93 MeV
0
20
40
60
80
100
120
140
θcm (DEGREES)

FIGURE 12

Angular distribution for the 17.64 MeV state transition, showing the fit obtained using potential $46W_V$.

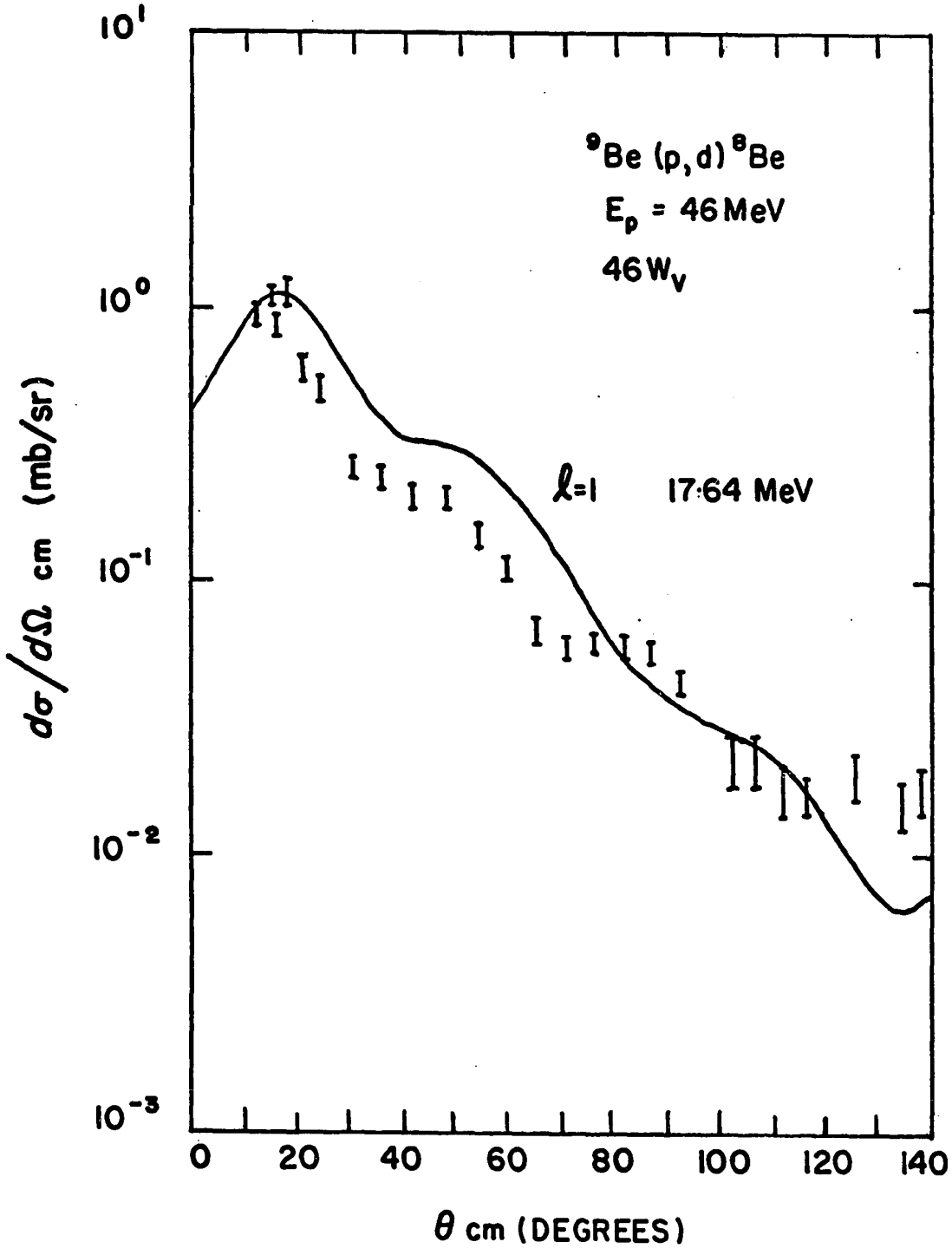
^{9}Be (p,d) ^{8}Be
E_p = 46 MeV
46 W_V
ℓ=1
17·64 MeV
$d\sigma/d\Omega$ cm (mb/sr)
θ cm (DEGREES)
10^{1}
10^{0}
10^{-1}
10^{-2}
10^{-3}
0
20
40
60
80
100
120
140

FIGURE 13

Angular distribution for the 17.64 MeV state transition, showing the fit obtained using potential $46W_D$.

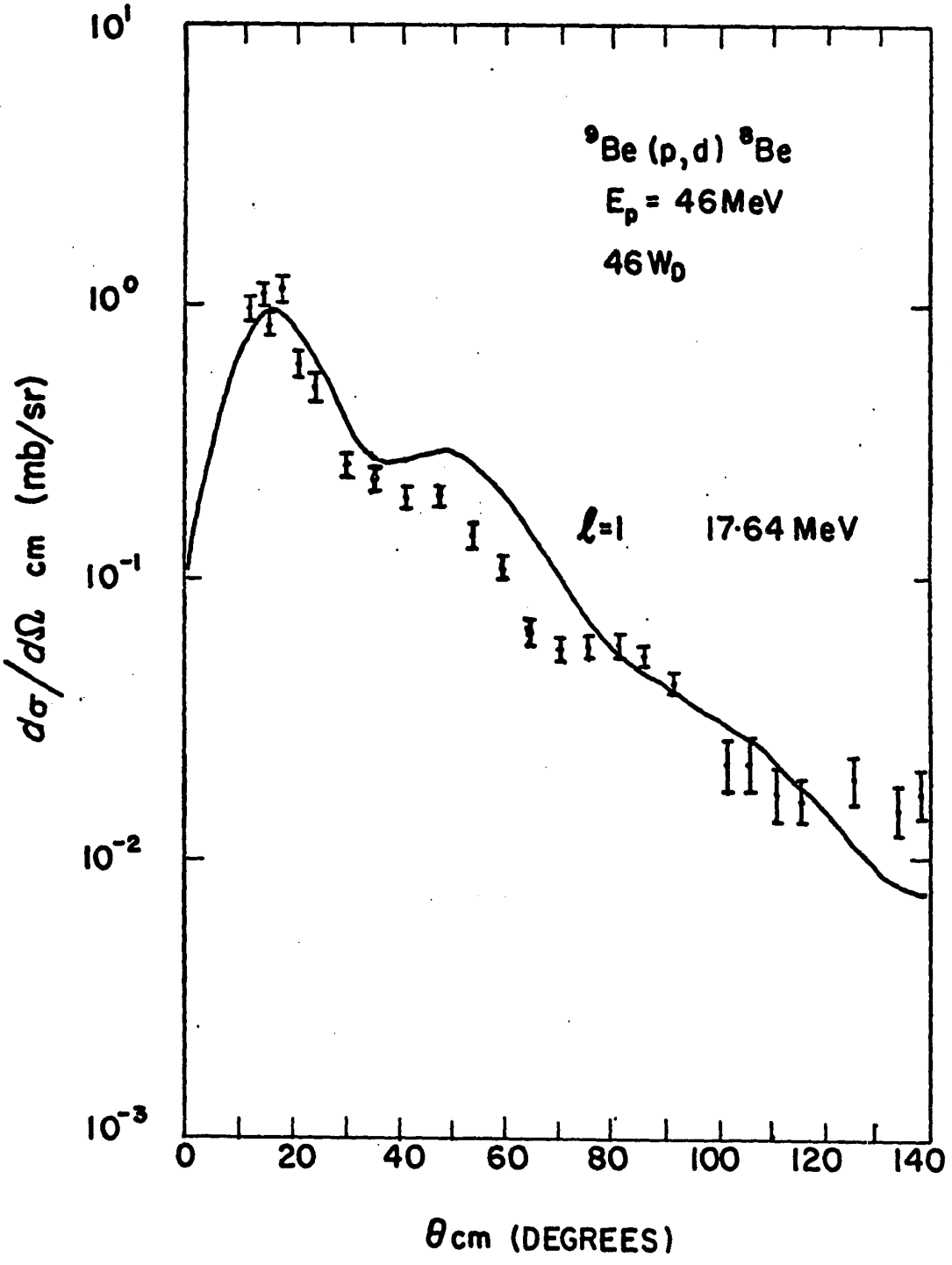
^{9}Be (p,d) ^{8}Be
E_p = 46MeV
46 W_D
ℓ=1
17·64 MeV
$d\sigma/d\Omega$ cm (mb/sr)
θcm (DEGREES)
10^{1}
10^{0}
10^{-1}
10^{-2}
10^{-3}
0
20
40
60
80
100
120
140

FIGURE 14

Angular distribution for the 13.15 MeV state transition, showing the fit obtained using potential $46W_V$.

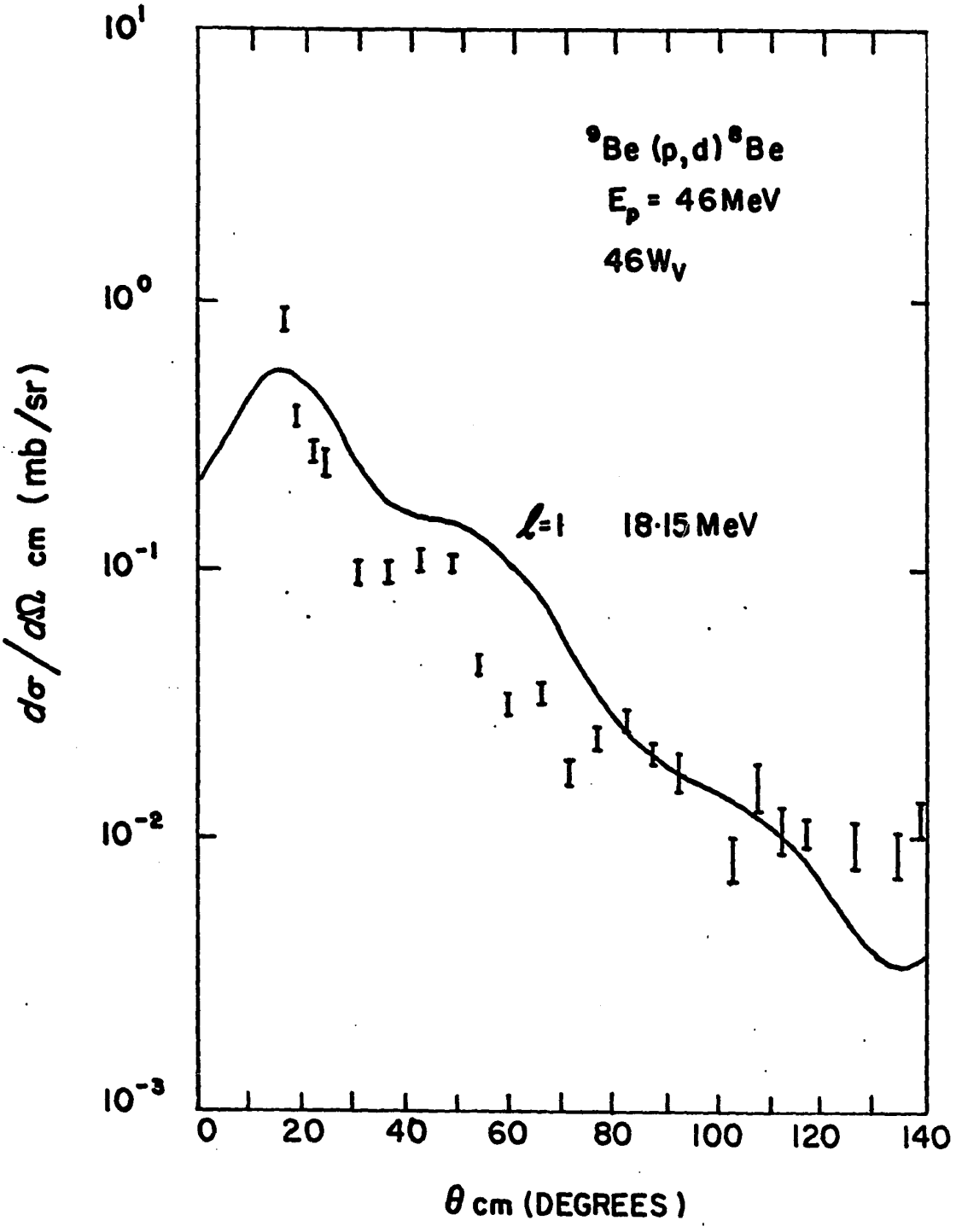
^{9}Be (p,d) ^{8}Be
E_p = 46MeV
46W$_V$
ℓ=1 18·15MeV
$d\sigma/d\Omega$ cm (mb/sr)
θ cm (DEGREES)
10^{1}
10^{0}
10^{-1}
10^{-2}
10^{-3}
0
20
40
60
80
100
120
140

FIGIRE 15

Angular distribution for the 18.15 MeV state transition, showing the fit obtained using potential $46W_D$.

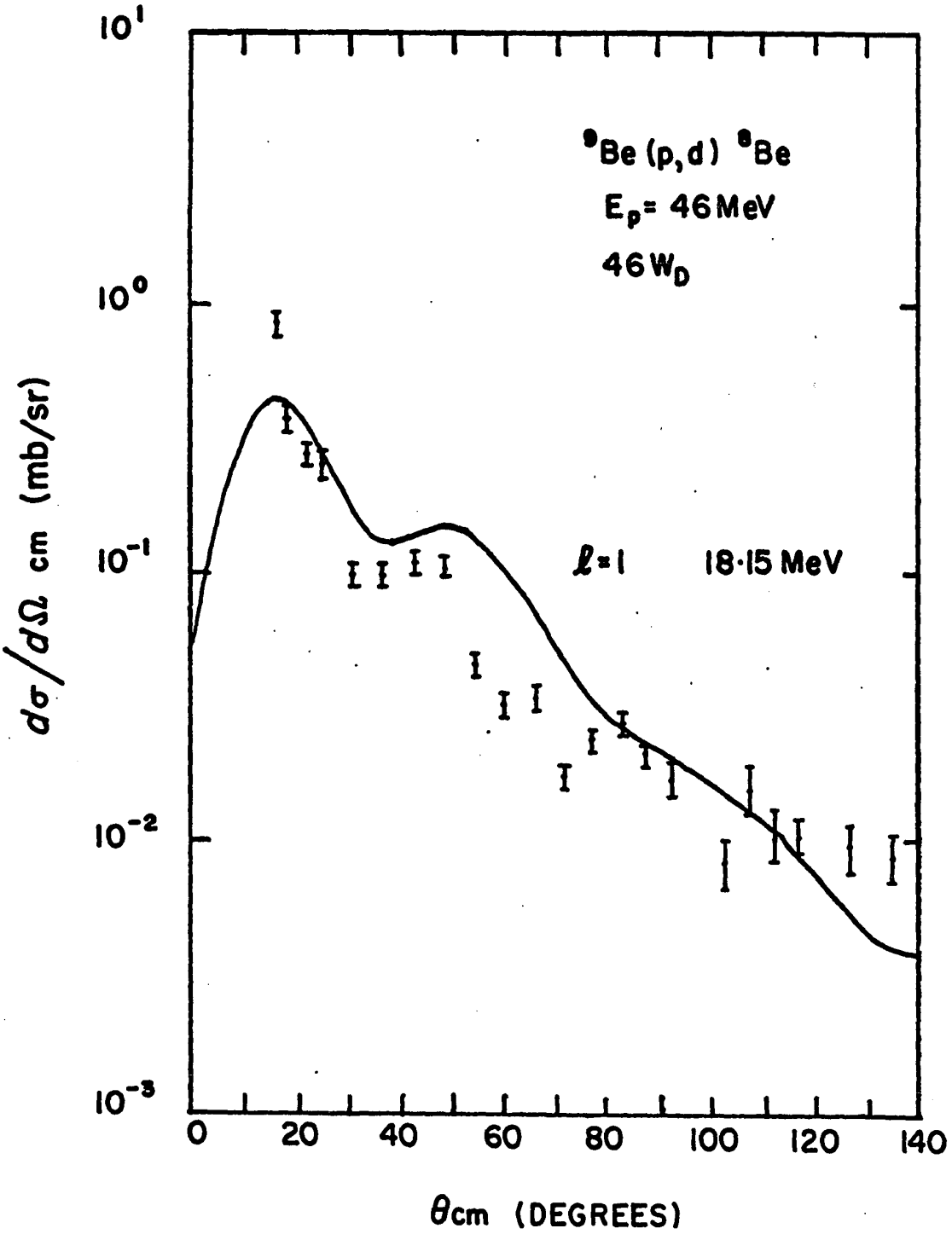
^{9}Be (p,d) ^{8}Be
E_p= 46 MeV
46 W_D
ℓ=1
18·15 MeV
$d\sigma/d\Omega$ cm (mb/sr)
θcm (DEGREES)
10^1
10^0
10^{-1}
10^{-2}
10^{-3}
0
20
40
60
80
100
120
140

FIGURE 16

Angular distribution for the 19.05 MeV state transition, showing the fit obtained using potential $46W_V$.

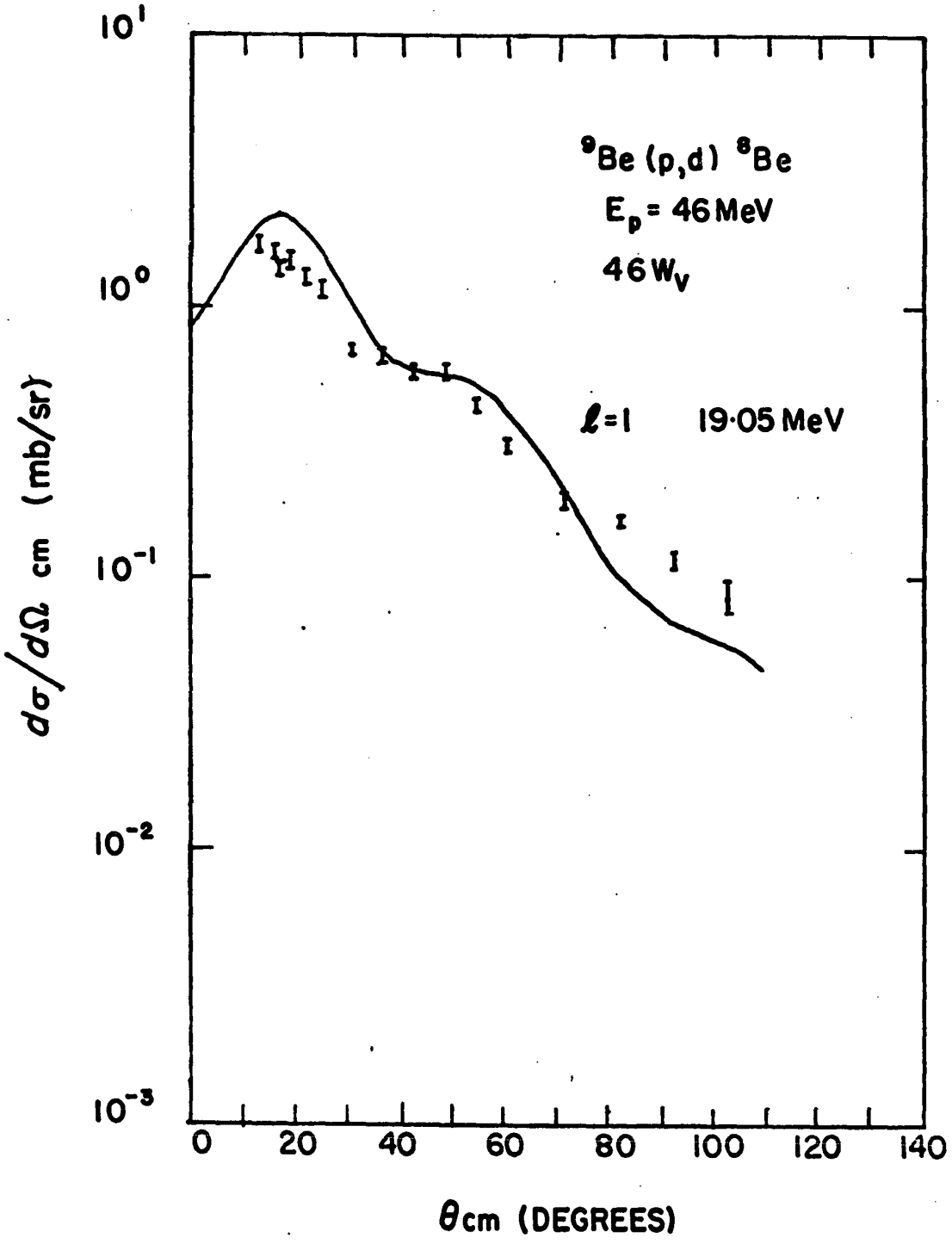
^{9}Be (p,d) ^{8}Be
E_p = 46 MeV
46 W_V
ℓ=1 19·05 MeV
10^1
10^0
10^{-1}
10^{-2}
10^{-3}
$d\sigma/d\Omega$ cm (mb/sr)
0 20 40 60 80 100 120 140
θcm (DEGREES)

FIGURE 17

Angular distribution for the 19.05 MeV state transition, showing the fit obtained using potential $46W_D$.

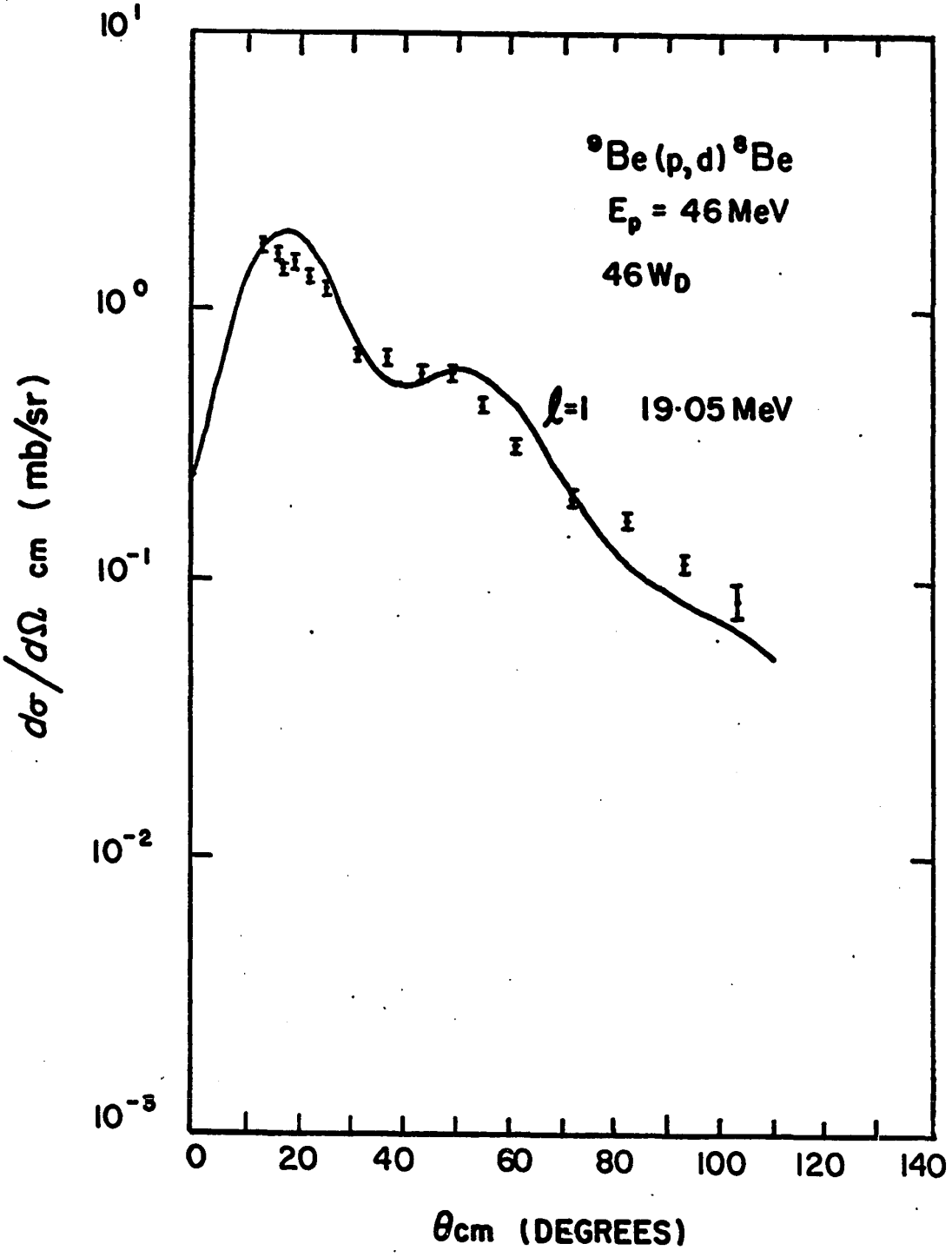
^{9}Be (p, d) ^{8}Be
E_p = 46 MeV
46 W_D
ℓ=1 19·05 MeV
$d\sigma/d\Omega$ cm (mb/sr)
θcm (DEGREES)
10^1
10^0
10^{-1}
10^{-2}
10^{-3}
0
20
40
60
80
100
120
140

FIGURE 18

Angular distribution for the 2.9 MeV state transition, showing the fit obtained using potential $100W_V$.

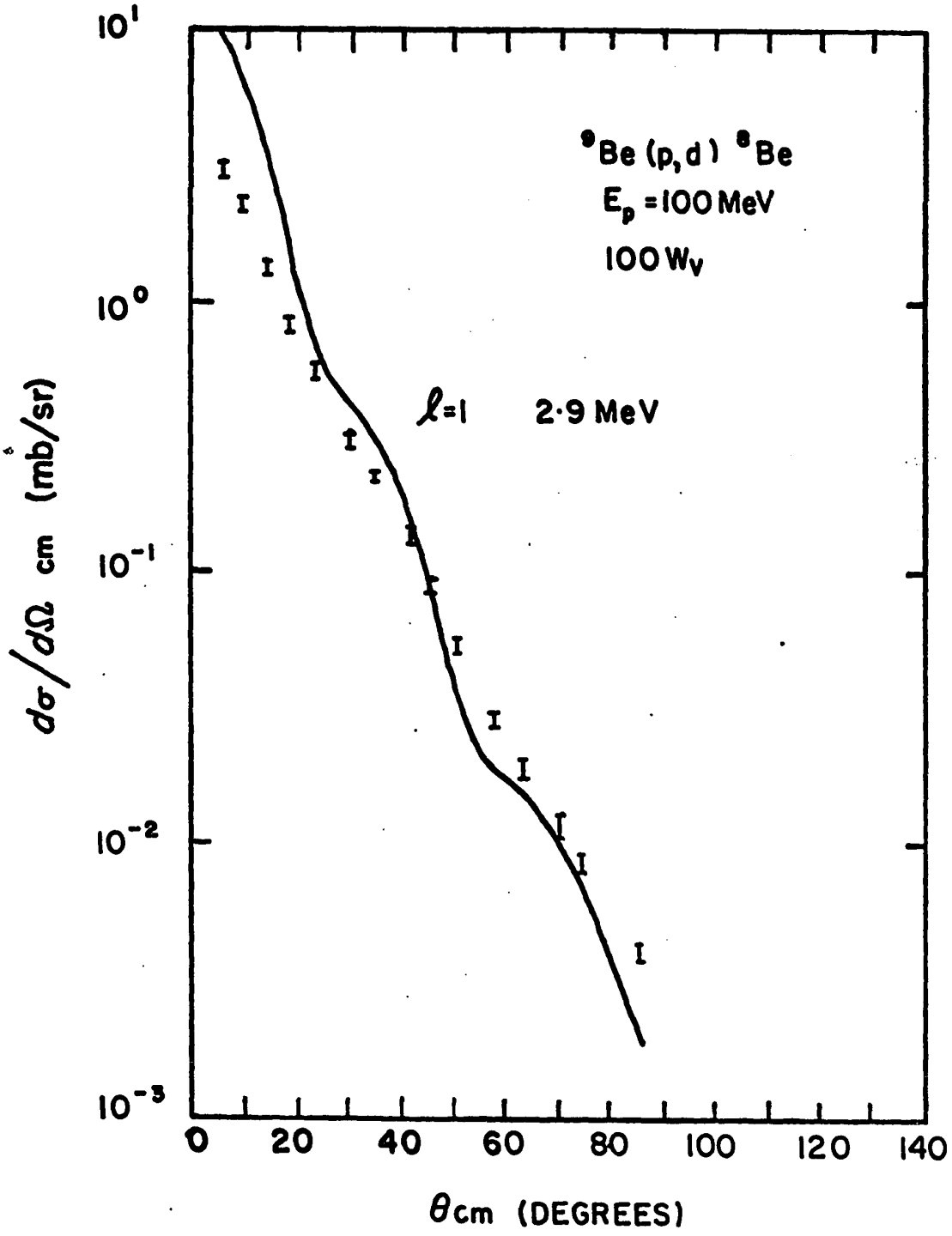
^{9}Be (p, d) ^{8}Be
E_p = 100 MeV
100 W_V
ℓ=1 2·9 MeV
$d\sigma/d\Omega$ cm (mb/sr)
θcm (DEGREES)
10^1
10^0
10^{-1}
10^{-2}
10^{-3}
0
20
40
60
80
100
120
140

FIGURE 19

Angular distribution for the 2.9 MeV state transition, showing the fit obtained using potential $100W_D$.

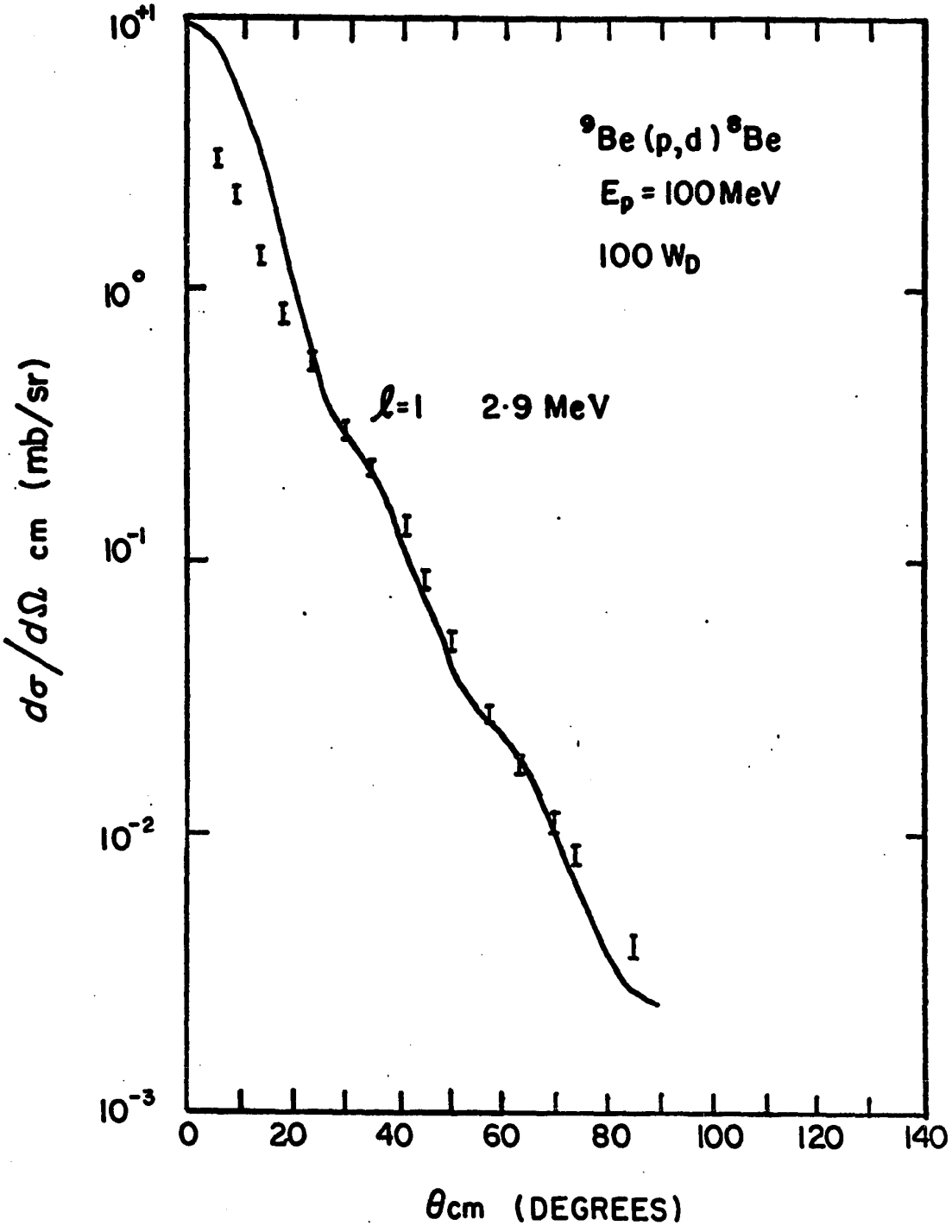
^{9}Be (p,d) ^{8}Be
E_p = 100 MeV
100 W_D
ℓ=1 2·9 MeV
$d\sigma/d\Omega$ cm (mb/sr)
θcm (DEGREES)
10^{+1}
10^{0}
10^{-1}
10^{-2}
10^{-3}
0
20
40
60
80
100
120
140

FIGURE 20

Angular distribution for the 16-20 MeV states transitions, showing the fit obtained using potential $100W_V$.

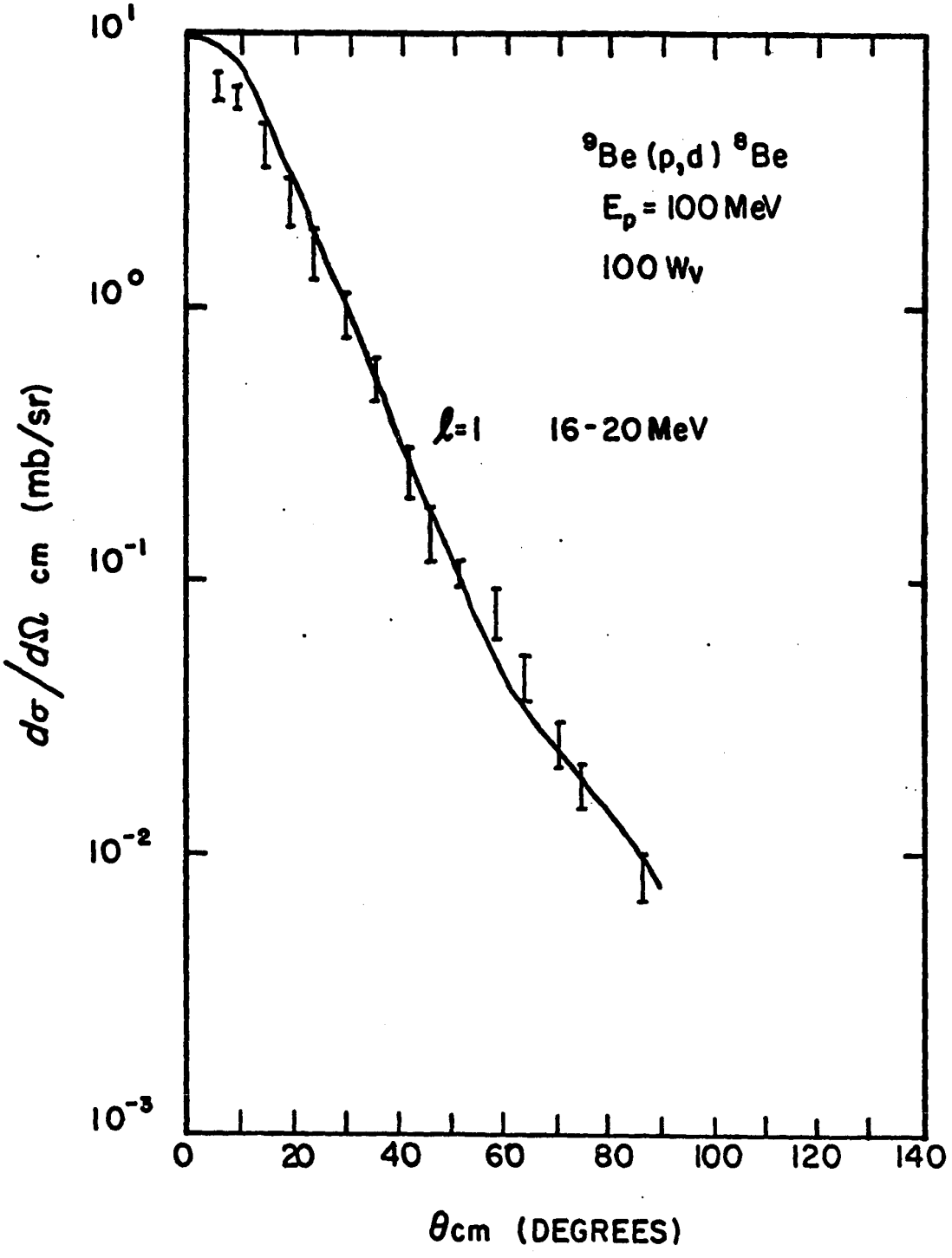
^{9}Be (p,d) ^{8}Be
E_p = 100 MeV
100 W_V
ℓ=1 16-20 MeV
$d\sigma/d\Omega$ cm (mb/sr)
θcm (DEGREES)
10^{1}
10^{0}
10^{-1}
10^{-2}
10^{-3}
0
20
40
60
80
100
120
140

FIGURE 21

Angular distribution for the 16-20 MeV states transitions showing the fit obtained using potential $100W_D$.

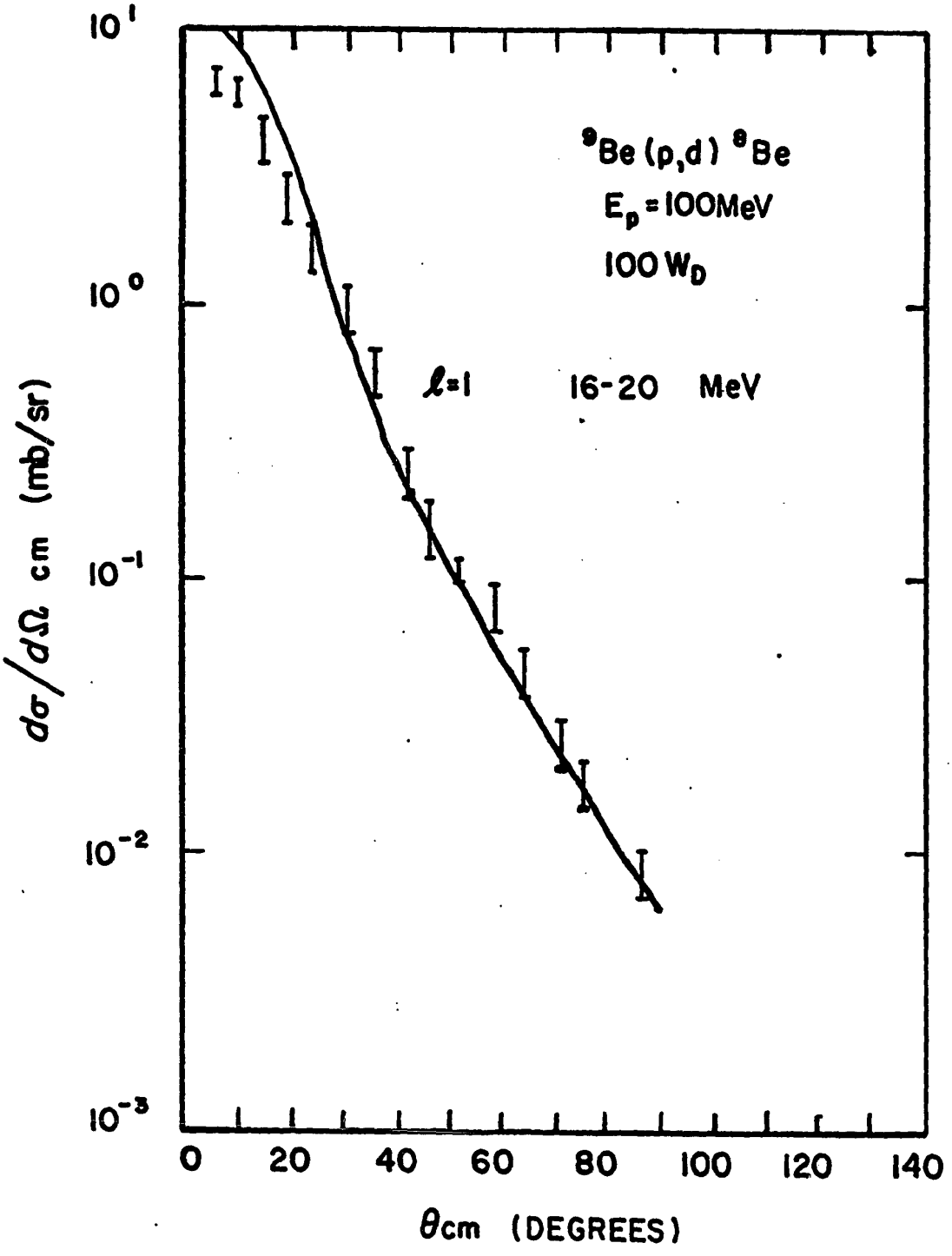
^{9}Be (p,d) ^{8}Be
E_p = 100MeV
100 W_D
ℓ=1
16-20 MeV
$d\sigma/d\Omega$ cm (mb/sr)
θcm (DEGREES)
10^1
10^0
10^{-1}
10^{-2}
10^{-3}
0
20
40
60
80
100
120
140

though. Hence, there is no inconsistency between the pairs of potentials.

In recent years several models have been proposed to explain the reaction $^{9}Be(p,d)\,^{8}Be$. For the 0.0, 2.9 and 11.4 MeV states of ^{8}Be, Wildermuth (1962) has proposed a cluster model in which two α-particles in ^{8}Be appear in the 0^{+}, 2^{+}, 4^{+} rotational sequence. In ^{9}Be, the additional neutron is loosely bound to the α-particles, and can be easily picked up leading to the excitation of the states of ^{8}Be (Jacmart et al., 1964). For the next group of states, from 16.63 to 19.22 MeV, this simple model breaks down. At 17.252 and 18.896 MeV ^{8}Be reaches the thresholds for break up into $^{7}Li + p$ and $^{7}Be + n$, respectively, (Lauritsen and Ajzenberg-Selove, 1966). Marion (1965) has proposed that the 2^{+} doublet at 16.63 and 16.93 MeV can be constructed from relatively pure single particle cluster states: Namely, the 16.63 MeV state is written $p + {}^{7}Li(gs)$ and the 16.93 MeV $n + {}^{7}Be(gs)$. Consider the ground state of ^{9}Be to be represented by $\alpha+\alpha+n$, and ^{7}Li and ^{7}Be, respectively, by $\alpha+t$ and $\alpha+{}^{3}He$. If the neutron is picked up from one of the α-particles, only ^{3}He and never t can be formed. Hence, the 16.63 MeV state should not be excited. In fact, the experimental results seem to bear out this conclusion (Marion et al., 1966; Kull, 1967; Verba et al., 1967). As a further extension of this model Marion (1965) proposed similar configurations

for the 1^+ doublet at 17.64 and 18.15 MeV. However, the magnitudes for the cross sections to these states are quite similar (Kull, 1967; Verba et al., 1967), which casts doubt on their interpretation as pure single particle cluster states.

A consequence of Marion's interpretation of the 16.63 and 16.93 MeV states is that they have isospin mixing of T = 0 and 1. For the nearly pure single particle states that Marion postulates, the mixture should be almost equal for each value of T. It is also thought (Kull, 1967) that the 1^+ doublet (17.64 and 18.15 MeV) and a possible 3^+ doublet (19.05 and 19.22 MeV) should exhibit isospin mixing. For this reason, the analysis of the states of the region 16.63 - 19.22 MeV was performed allowing different mixtures of isospin from pure T = 0 to pure T = 1 to be incorporated into the calculated differential cross sections.

Tables 4-6 and 4-7 show the spectroscopic factors extracted from fitting the two sets of data. Also, the intermediate coupling shell model spectroscopic factors of Cohen and Kurath (1967) and Balashov et al., (1965) are displayed for comparison. In the case of the 16.93 to 19.05 MeV states, spectroscopic factors were calculated assuming both pure T = 1 and pure T = 0. Hence, the values for these states can easily be found if the proper isospin mixture is known. In the case of the 16-20 MeV

TABLE 4-6

Spectroscopic factors extracted in this work, compared to theoretical results.

State	J^π	T	$S_{1/2}$	$S_{3/2}$	S	Potential
0.0	0^+	0		$.724 \pm .224$	$.724 \pm .224$	$46W_V$
2.9	2^+	0	$.145 \pm .033$	$1.641 \pm .375$	$1.786 \pm .376$	
16.93	2^+	0	$.236 \pm .104$	$.987 \pm .435$	$1.223 \pm .435$	
		1	$.370 \pm .163$	3.263 ± 1.44	$1.211 \pm .482$	
17.64	1^+	0	$.211 \pm .117$	$.078 \pm .043$	$.289 \pm .125$	
		1	$.417 \pm .231$	$.434 \pm .241$	$.284 \pm .112$	
18.15	1^+	0	$.109 \pm .079$	$.040 \pm .029$	$.150 \pm .084$	
		1	$.217 \pm .157$	$.226 \pm .164$	$.140 \pm .076$	
19.05	(3)	0		$.545 \pm .197$	$.545 \pm .197$	
		1		$1.634 \pm .590$	$.545 \pm .197$	
0.0	0^+	0		$.660 \pm .224$	$.660 \pm .224$	$46W_D$
2.9	2^+	0	$.126 \pm .031$	$1.424 \pm .354$	$1.549 \pm .355$	
16.93	2^+	0	$.206 \pm .067$	$.860 \pm .279$	$1.066 \pm .287$	
		1	$.323 \pm .105$	$2.844 \pm .923$	$1.056 \pm .310$	
17.64	1^+	0	$.188 \pm .079$	$.069 \pm .029$	$.259 \pm .034$	
		1	$.371 \pm .156$	$.387 \pm .163$	$.253 \pm .075$	
18.15	1^+	0	$.096 \pm .060$	$.035 \pm .022$	$.131 \pm .064$	
		1	$.191 \pm .120$	$.199 \pm .125$	$.130 \pm .068$	
19.05	(3)	0		$.529 \pm .125$	$.529 \pm .125$	
		1		$1.587 \pm .374$	$.529 \pm .125$	
0.0	0^+	0		.5800[a]	.369[b]	
2.9	2^+	0	.0588[a]	.6663	.713	
16.93	2^+	0	.0830	.3465	.346	
		1	.1528	1.3461	.401	
17.64	1^+	0	.0423	.0156	.069	
		1	.2965	.3091	.198	
18.15	1^+	0	.0423	.0156	.069	
		1	.2965	.3091	.198	
19.05	(3)	0		.1076	.151	
		1		.5260	.113	

a) Cohen and Kurath, 1967
b) Balashov et al., 1965

TABLE 4-7

Spectroscopic factors extracted in this work.

State	J^π	T	$S_{1/2}$	$S_{3/2}$	S	Potential
0.0	0^+	0		.602±.418	.602±.418	$100W_V$
2.9	2^+	0	.113±.053	1.276±.602	1.388±.604	
16.93	2^+	0	.181±.043	.755±.172	.936±.178	
		1	.283±.065	2.495±.570	.926±.191	
17.64	1^+	0	.282±.064	.104±.024	.386±.069	
		1	.549±.125	.573±.131	.374±.060	
18.15	1^+	0	.282±.064	.104±.024	.386±.069	
		1	.549±.125	.573±.131	.374±.060	
19.05	(3)	0		.325±.074	.325±.074	
		1		.975±.223	.325±.074	
0.0	0^+	0		.674±.190	.674±.190	$100W_D$
2.9	2^+	0	.094±.033	1.070±.373	1.165±.375	
16.93	2^+	0	.098±.024	.409±.102	.507±.121	
		1	.154±.038	1.354±.337	.503±.113	
17.64	1^+	0	.152±.038	.056±.014	.208±.040	
		1	.293±.074	.311±.077	.203±.036	
18.15	1^+	0	.152±.038	.056±.014	.208±.040	
		1	.293±.074	.311±.077	.203±.036	
19.05	(3)	0		.176±.044	.176±.044	
				.529±.132	.176±.044	

group at 100 MeV, the analysis is not very dependable. Besides the assumption that j = 1/2 and 3/2 components of the scattering follow the relative values from Cohen and Kurath, it was necessary to assume that the relative strengths among the four states could be found using the values given by Cohen and Kurath. In addition, the four contributing states were added together assuming either pure T = 0 or pure T = 1.

Comparing the extracted spectroscopic factors to Cohen and Kurath's, it is apparent that there are large differences. For the ground state, the values agree within the assigned error. However for the excited states, the extracted values are in many cases from two to five times larger than Cohen and Kurath's values. In the case of the ground state, one would expect agreement with CCohen and Kurath since their value was used in the search to obtain order-of-magnitude agreement with the data. If the intermediate coupling model used to compute the spectroscopic values were a good description of ^{9}Be, there should be fair agreement between the computed and extracted values for the excited states. The lack of such agreement casts doubt on the validity of the model. Similarly, comparison with Balashov's values for shows marked discrepancy between the extracted and predicted results. It seems that neither intermediate coupling calculation reflects the structure of ^{9}Be very accurately.

Two other investigators have extracted spectroscopic factors from $^{9}Be(p,d)\,^{8}Be$ at 33.6 MeV (Kull, 1967) and 155 MeV (Towner; 1969). Table 4-8 shows the results of this work compared to those of Towner. The quantity given as $\mathcal{S}$ is $\mathcal{S}_{1/2}+\mathcal{S}_{3/2}$ for T = 0 and $\frac{1}{3}(\mathcal{S}_{1/2}+\mathcal{S}_{3/2})$ for T = 1. For the ground and 2.9 MeV states, the extracted values are in fair agreement, but for the higher states, the results of this work are systematically higher than those extracted by Towner. Kull appears to get fairly good agreement with Cohen and Kurath by calculating his spectroscopic factors with isospin mixing included. From the figure showing his fit to the ground state transition, it appears that the quality of fitting in his work and in this one are comparable. In conclusion, it would seem that the results presented here are less encouraging for Cohen and Kurath's model than are those of either Kull or Towner. It is important to note that the experimental results analyzed by Towner covered an angular range from about 4° to 35°. This makes his analysis less reliable.

TABLE 4-8

Spectroscopic factors extracted by Towner (1969) for comparison to the values given in tables 4-6 and 4-7.

State	J^π	T	S
0.0	0^+	0	$.50 \pm .14$
2.9	2^+	0	$.99 \pm .17$
16.63	2^+		$.54 \pm .12$
16.93	2^+		
17.64	1^+		$.08 \pm .06$
18.15	1^+		
19.05	(3)		$.17 \pm .03$
19.22	3^+		

CHAPTER 5

CONCLUSION

A DWBA computer code has been developed by Dr. T.Y. Li for use in calculating the angular distribution in (p,d) and (p,α) reactions. The code has the advantage of being fairly simple to operate without a detailed knowledge of its construction and gives results in agreement with those obtained from similar analyses.

The first part of this paper deals with the formalism of direct reaction theory applied to the pick-up and stripping reactions. Some of the basic concepts involved in calculating spectroscopic factors in the J T representation are also discussed. Since the basic problem of DWBA is to generate and integrate over the distorted waves and bound state wave function, a good deal of time is spent on the numerical analysis of these functions. Special attention is paid to the zero-range and finite-range approximations.

After the theory has been explained, it is used to analyze angular distributions from ^{9}Be(p,d) ^{8}Be at 46 MeV and 100 MeV. Proton optical potentials were obtained from elastic scattering data and deuteron optical potentials were found by optimizing the fitting to the angular distribution of the ground state transition in the (p,d) reaction. The potentials thus obtained are in general agreement with the results of optical model analysis at other energies.

These potentials were used to analyze the transitions to the excited states. The quality of fits to the various states observed in the reaction is fairly good. From these fits it has been possible to extract a fairly extensive table of spectroscopic factors, which appears in tables 4-6 and 4-7. The extracted results are compared to those of Towner (1969) and Kull (1967). Both these authors claim fair agreement with the intermediate coupling calculations done by Cohen and Kurath (1967). The present work is compared with Towner's results in table 4-8 and sizable discrepancy has been observed except for the ground and 2.90 MeV states. Comparison with Cohen and Kurath's values for the spectroscopic factors leads to some doubts about the validity of their model for ^{9}Be. The same statement applies to the calculation of Balashov et al. (1965).

Other investigators have had some success using various cluster arrangements to describe ^{9}Be. Jacmart (1964) uses two α-particles with a loosely bound neutron to describe the energy levels of ^{9}Be. Marion (1965) and Marion et al. (1966) have been successful in describing ^{9}Be(p,d) ^{8}Be transitions to the 16.63 and 16.93 MeV states using the configurations p + ^{7}Li(gs) and n + ^{7}Be(gs). This model also gives isospin mixing for T = 0, and 1 in the states, which seems to be reasonable. The pair of states at 17.64 and 18.15 MeV has been tentatively identified with similar configurations involving the first excited states

of ^{7}Li and ^{7}Be. These designations, however, have not met with as much success as the others. Generally speaking, the cluster approach seems in some respects to be more suitable than the shell model. It would be interesting to see what kind of spectroscopic factors such a model yields.

Since the present work was begun, the DWBA code has been expanded by Dr. T.Y. Li to include spin-orbit potentials in both channels with a search facility in the deuteron channel. A very rough preliminary calculation indicates that further investigation of this modification could be fruitful. In addition, the optical model code has been modified so that the real and spin-orbit diffusenesses are coupled to the real and spin-orbit radii through the size of the root-mean-square nuclear radius. There has not yet been time to investigate the effect on the quality of fitting of these additional constraints, but it is hoped that this will soon be possible. In addition, there are further data from ^{16}O(p,d) ^{15}O at 100 MeV to be analyzed. This work should be completed within the next few months and the results can be made known.

REFERENCES

ABRAMOWITZ, M., AND I. A. STEGUN, Handbook of mathematical Functions, National Bureau of Standards, Report No. AMS 55 (1965).

BALASHOV, V. V., A. N. BOYARKINA, AND I. ROTTER, Nucl. Phys. 59 (1965) 417.

BASSEL, R. H., R. M. DRISKO, AND G. R. SATCHLER, Oak Ridge National Laboratory Report ORNL-3240, unpublished.

BLATT, J. M. AND V. F. WEISSKOPF, Theoretical Nuclear Physics (Wiley, 1952).

BRINK, D. M. AND G. R. SATCHLER, Angular Momentum (Oxford University Press, 1968).

BUTLER, S. T. AND C. H. HITTMAIR, Nuclear Stripping Reactions (Wiley, 1957).

BUTTLE, P. J. A. AND L. J. B. GOLDFARB, Proc. Phys. Soc. 83 (1964) 701.

CARLSON, R. F. ET AL., Bull. Am. Phys. Soc. 12 (1967) 483.

COHEN, S. AND D. KURATH, Nucl. Phys. A101 (1967) 1.

DE-SHALIT, A. AND I. TALMI, Nuclear Shell Theory (Academic Press, 1963).

EDMUNDS, A. R., Angular Momentum in Quantum Mechanics (Princeton University Press, 1960).

EDMONDS, A. R. AND B. H. FLOWERS, Proc. Roy. Soc. (London) A214 (1952) 512.

FESHBACH, H,, Annals of Phys. 5 (1958) 237.

FLOWERS, B. H., Proc. Roy. Soc. (London) A212 (1952) 248.

GELL-MANN, M., AND M. L. GOLDBERGER, Phys. Rev. 91 (1953) 398.

GLENDENNING, N. K., Ann. Rev. Nucl. Sci. 13 (1963) 191.

HOUDAYER, A., M. Sc. thesis McGill University (1969).

JACMART, J. C., J. P. GARRON, M. RIOU, AND C. RUHLA, Phys. Lett. 8 (1964) 269.

JAHN, H. A., Proc. Roy. Soc. (London) A201 (1950) 516.

JAHN, H. A. AND H. VAN WIERINGEN, Proc. Roy. Soc. (London) A209 (1951) 502.

KULL, L. A., Phys. Rev. 163 (1967) 1056.

LAURITSEN, T. AND F. AJZENBERG-SELOVE, Nucl. Phys. 78 (1966) 1.

LEE, J. K. P., S. K. MARK, P. M. PORTNER, AND R. B. MOORE, Nucl. Phys. A106 (1967) 357.

LI, T. Y., Ph. D. thesis University of Manitoba (1967).

LI, T. Y. AND S. K. MARK, Can. Jour. Phys. 46 (1968) 2645.
Can. Jour. Phys. 47 (1969a) 257.
Nucl. Phys. A123 (1969b) 147.

MAC FARLANE, M. H. AND J. B. FRENCH, Revs. Mod. Phys. 32 (1960) 567.

MARION, J. B., Phys. Lett. 14 (1965) 315.

MARION, J. B., C. A. LUDEMANN, AND P. G. ROOS, Phys. Lett. 22 (1966) 172.

MARK, S. K., Ph. D. thesis McGill University (1965).

MESSIAH, A., Quantum Mechanics (Wiley, 1966).

MILNE, W. E., Numerical Calculus (Princeton University Press, 1962).

NIGAM, B. P. AND R. R. ROY, Nuclear Physics (Wiley, 1967).

SATCHLER, G. R., Nucl. Phys. A100 (1967) 481.

SMITH, W. R., Oak Ridge National Laboratory Report ORNL-TM-1151, unpublished.

TOBOCMAN, W., Theory of Direct Nuclear Reactions (Oxford University Press, 1961).

TOWNER, I. S., Nucl. Phys. A126 (1969) 97.

VERBA, J. W. ET AL., Phys. Rev. 153 (1967) 1127.

WILDERMUTH, K., Nucl. Phys. 31 (1962) 478.

APPENDIX A

SIMPLIFICATION OF $|T_{if}|^2$

Simplification of equation 2-39 involves the use of the symmetry and orthogonality relations for the Clebsch-Gordon and Wigner coefficients (Brink and Satchler, 1968). Each of the three pairs of Clebsch-Gordon coefficients must be treated separately and in the order shown in what follows.

First,

$$\sum_{M_i M_f} \langle J_f M_f | J_i M_i \, j' m_j' \rangle \langle J_i M_i \, j m_j | J_f M_f \rangle = \left(\frac{2J_f+1}{2j+1}\right) \delta_{jj'} \delta_{m_j m_j'} \quad \text{(A-1)}$$

Now that the equalities $j=j'$ and $m_j=m_j'$ have been found, the rest is easy. Directly, one sees that the sum over projectile spins leads to

$$\sum_{\mu_d \mu_p} \langle \tfrac{1}{2} \mu_p \tfrac{1}{2} m_s' | | \mu_d \rangle \langle | \mu_d | \tfrac{1}{2} \mu_p \tfrac{1}{2} \mu_s \rangle = \tfrac{3}{2} \delta_{m_s m_s'}. \quad \text{(A-2)}$$

This reduction leads to the equality $m_s=m_s'$, so finally the last pair of coefficients can be simplified.

$$\sum_{m_j m_s} \langle l' m_l' \tfrac{1}{2} m_s | j m_j \rangle \langle j m_j | l m_l \tfrac{1}{2} m_s \rangle = \left(\frac{2j+1}{2l+1}\right) \delta_{ll'} \delta_{m_l m_l'} \quad \text{(A-3)}$$

When all these simplifications are substituted into equation 2-39, the new expression is

$$\sum_{\substack{M_i M_f \\ \mu_p \mu_d}} |T_{if}|^2 = \frac{3 \langle T_i M_{T_i} \tfrac{1}{2} \tfrac{1}{2} | T_f M_{T_f} \rangle^2}{4} (2J_f+1) \sum_{j l m_l} |\beta_{lj}|^2 |\beta_l^{m_l}|^2. \quad \text{(A-4)}$$

Equation 2-40 is found by adding the results of anti-symmetrization and using the definition of the differential cross section.

APPENDIX B

USE OF THE DWBA COMPUTER CODE

The DWBA code is designed for use on the IBM 360 series of computers. It requires 220 K memory to run. Below will be listed a card-by-card outline of the input data, followed by a list of the options available with the code.

Card #1: Format 8F10.3

T(1)-Laboratory energy of the incident particle, given in MeV.

T(2)-Q-value if the reaction, given in MeV.

T(4)-Mass of the target nucleus, given in AMU.

T(20)-Mass of the incident particle, given in AMU.

T(21)-Mass of the outgoing particle, given in AMU.

T(3)-Charge number (Z) of the target.

SPECTR-Theoretical spectroscopic factor.

BETA-Deformation parameter for a deformed Woods-Saxon potential. It may be either positive or negative, and is 0 for no deformation.

Card #2: Format 8F10.3

T(22)-Mass of the stripped or picked-up particle, given in AMU.

T(24)-Charge number for the outgoing particle.

T(25)-Charge number for the incident particle.

T(5)-Orbital angular momentum of the bound state of the bound particle.

XR(1)-Radius parameter for the Woods-Saxon potential of the bound particle, given in fm.

XA(1)-Difuseness parameter the Woods-Saxon potential of the bound particle, given in fm.

T(8)-$2J_f+1/2J_i+1$. It is necessary only in (d,p) calculations, but should not be set to 0.

T(13)-Calls finite-range or zero-range option. It must be small, about .000001. See more details under options.

Card #3: Format 8F10.3

T(14)-Maximum number of partial waves to be used. As many as 50 partial waves are available.

T(15)-Number of radial nodes in the bound state wave function, not counting the origin.

T(16)-Increment used in integration. Increments of about .1fm have proven satisfactory in the past.

T(17)-Wave number used in the (p,α) reaction. Use .231605/fm.

T(18)-Square well radius used in the (p,α) reaction. Use 2.7835fm.

T(19)-Wave number related to the square well depth used in the (p,α) reaction. Use .8186/fm.

T(23)-Binding energy of either the deuteron or the α-particle, depending on the reaction. It is given in MeV.

XMU-Simple harmonic oscillator parameter used in the (p,α) reaction. Use .05429.

Card #4: Format 8F10.3

TY1-Coulomb radius for the incident particle, given in fm.

TY2-Coulomb radius for the outgoing particle, given in fm.

XV(1)-Spin-orbit well depth for the bound particle, given in MeV.

T(10)-Interior cutoff radius of the bound particle. It is not used, so set to 0.

T(9)-Number of the experimental point to which the cross sections are normalized. It can range from 1 to the maximum number of data points used in the calculation.

T(11)-Set to 0.

T(12)-Set to 0. Neither this nor the item above are any longer necessary in the program.

RCX-Coulomb radius of the bound particle.

Card #5: Format 4F10.3

This card contains the Woods-Saxon radius parameters for both channels, given in fm, as well as the diffusenesses, also in fm, for the real potential term. The order is incident channel radius, outgoing channel radius, incident channel diffuseness, and outgoing channel diffuseness.

Card #6: Format 4F10.3

The same order as used in card #5 is used to display the imaginary potential radii and diffusenesses. For further details, see the options.

Card #7: Format 6F10.3

The potential depths for both channels are read in in the order incident channel real, outgoing channel real, incident volume imaginary, outgoing volume imaginary, incident surface imaginary, and outgoing surface imaginary. All potentials are read in with positive signs, and those not involved must be set to 0.

The order of cards given so far applies if there are no data. If there are data, cards numbered 4a and 4b are inserted between cards 4 and 5, and 8, 9, and10 come after 7.

Card #4a: Format I4

This card merely indicates the number of experimental points listed on the card(s) which follow.

Card #4b: Format 9F8.0

Data are listed on as many cards as is necessary at three points to the card. The listing is angle in degrees, cross section in mb/sr, and error for the measurement in mb/sr.

Card #8: Format I4

Indicate the number of points desired in the automatic search. If none, put 0; if more, there is no upper limit except the number the computer will accept. For sufficiently large values, for instance 100, the job will run until allocated time is used.

Card #9: Format 17I3

Indicate which parameters are to be varied in

the automatic search. The code is 1 for a parameter to be varied independently, 0 for a parameter not to be varied, and -N for a parameter to take the value assigned to parameter N. The seventeen spaces of I format are allotted, one to a parameter in the following order: 1-5 are allotted to radius parameters. Bound particle, incident channel real, incident channel imaginary, outgoing channel real, and outgoing channel imaginary. 6-10 are allotted to the diffusenesses using the same order as used for the radii. 11-17 are allotted to the potential parameters in the order bound particle spin-orbit, incident channel real, incident channel volume imaginary, outgoing channel real, outgoing channel volume imaginary, incident channel surface imaginary, and outgoing channel surface imaginary.

Card #10: Format I3

Indicate the number of independently varied parameters. If a number on card 9 is negative, the parameter is not independently varied.

OPTIONS

Card #1:

T(1)-If negative, the set of data in which it appears is the last to be read. When the calculation is completed, the job is finished.

T(4) and T(20)- In conjunction with XR(1) from card 2, these parameters indicate which of the reactions

(p,d), (d,p), and (p,α) is to be calculated. If T(4) is positive, the (p,α) reaction is done; if T(4) is negative and XR(1) is positive, (d,p) is calculated; and if T(4) is negative and XR(1) is negative, (p,d) is calculated. When (p,α) is done T(20) must be negative for ^{7}Li(p,α)α because of the use of Boson rather than Fermion statistics. For every other case, T(20) is positive.

SPECTR-If this is positive, χ^2 is calculated after normalizing the calculated angular distribution to the data. If it is negative, χ^2 is calculated before normalization.

Card #2:

T(5)-Indicate j=l+$\frac{1}{2}$ when this is positive, and j=l-$\frac{1}{2}$ when this is negative.

T(8)-No data need be supplied if this is positive. The angular distribution is the calculated at 5 intervals from 0 -180 . If T(8) is negative, experimental data must be supplied.

T(13)-For positive values, the finite range approximation is used; for negative values, the zero-range approximation is used.

Card #3:

T(17)-When the (p,α) reaction is calculated, simple harmonic oscillator wave functions are used in the finite range calculation if T(17) is negative. For positive values, square well wave functions are used.

Card #4:

RCX-If this is positive, assume RCX takes on the value of the incident channel real radius. If it is negative, the magnitude of the stated value of RCX is used. This is only important in the (p,α) reaction, since the neutron is not charged.

Card #5:

Outgoing channel diffuseness-When it is positive, the imaginary volume parameters are set equal to the real parameters, not including the well depths. When it is negative, the imaginary surface and volume geometrical parameters are set equal. In the negative option it is possible to distinguish volume and surface imaginary parameters as they are entered on cards 5 and 6.